Image Cover Sheet

CLASSIFICATION	SYSTEM NUMBER 59954
UNCLASSIFIED	

TITLE

DEVELOPMENT OF AN OPTICALLY PUMPED POTASSIUM SEARCH MODE MAGNETOMETER

System Number:

Patron Number:

Requester:

Notes:

DSIS Use only:

Deliver to: JR

89-02041
5995C

UNCLASSIFIED   UNLIMITED

DRES

CONTRACT REPORT 16/89

DEVELOPMENT OF AN
OPTICALLY PUMPED POTASSIUM
SEARCH MODE MAGNETOMETER

Scintrex Ltd.

Concord, Ontario

DEFENCE RESEARCH ESTABLISHMENT SUFFIELD, RALSTON, ALBERTA

"This work was carried out for DRES under contract. The accuracy
of the information presented herein is the responsibility solely of the
contractor and is NOT to be construed as an Official Department
of National Defence position unless so designated by other
authorizing documents."

UNCLASSIFIED

FINAL PROGRESS REPORT

DEVELOPMENT OF AN OPTICALLY PUMPED
POTASSIUM SEARCH MODE MAGNETOMETER

DSS CONTRACT 8SG84-00028

Submitted By:

Scintrex Limited
222 Snidercroft Road
Concord, Ontario
L4K 1B5

Telephone: (416) 669-2280
Telex: 06-964570
Telefax: (416) 669-5132
Cable: Geoscint Tor

RD/IB-3/14

TABLE OF CONTENTS

1

1.0   INTRODUCTION

The potassium search mode magnetometer was proposed as a potential means of reducing the problem of orientation error which is present in existing optically pumped alkali vapor magnetometers such as those based on cesium. Because the energy difference between adjacent Zeeman sublevels in the ground state are significantly different for each of the 4 possible transitions, it is possible to observe 4 distinct absorption lines in an optical pumping experiment in which an atomic vapor of potassium is oriented by circularly polarized D1 light. The lines can be resolved and therefore the transition frequencies can be accurately measured individually. If the line widths are small enough (say less than 5 nT) then frequency errors due to the superposition of adjacent lines (line interaction) are negligible. (see Section 4.3). Therefore if the relative intensities of the absorption lines change (as for example when the orientation angle between the pumping light and the magnetic field is changed) then there should be no significant frequency shift due to line interaction.

However, in the case of cesium there are 8 transition frequencies which are nearly identical. The line widths are comparable to the line separation which means that the individual lines cannot be resolved. What is observed is effectively a single composite absorption line. When the relative intensities of the lines change then so does the shape and effective centre frequency of the composite line. Thus a single beam cesium magnetometer has very severe orientation errors due to line interaction alone.

The split beam cesium magnetometer was developed to resolve this problem by applying equal amounts of left and right polarized D1 light to the absorption cell. This results in a composite line with which the symmetry about the line center is conserved under orientation change. The difficulty with this technique is in proper balancing of the amounts of left and right polarized light. This balancing procedure would not be required for a potassium magnetometer.

The effort to develop an optically pumped potassium search mode magnetometer was much larger than we anticipated. The progress was at times slow as many preparatory tasks had to be accomplished before the reliable experiments could be conducted. A reasonably long lasting lamp had to be developed as described in Section 5. A prolonged development was required to establish the absorption cell optimal pressure and most suitable buffer gas (Section 4.1.). Investigation of resonant line interaction had to be completed to gain knowledge of what are the minimum requirement for the resonant line linewidth (Section 4.2 and 4.3). A complex and very precise experimental set up had to be developed (Section 5) before the major task of orientation error determination and reduction could start. A series of long orientation error measurements (Section 7) culminated in the revelation that the orientation errors are rather large and no simple means or reasonable tradeoffs could be devised to reduce them to the acceptable level. In parallel with the orientation error measurements the investigation of different magnetometer embodiment was conducted (Section 9). The potential of the potassium magnetometer was reassessed (Section 10) and the conclusions deducted (Section 11).

2.0 OPERATING PRINCIPLES AND PERFORMANCE CHARACTERISTICS

2.1 Operating of the Self-Oscillating Magnetometer

The principle of operation of an optically pumped magnetometer is based on the Zeeman effect, which shows that certain characteristic atomic frequencies are magnetic field dependent. They can be measured utilizing the resonant response of an atomic system (such as atomic potassium vapour) subjected to the static magnetic field H_0 to be measured (for example earth's magnetic field) generally in the presence of an auxiliary oscillating field H_1 (called ratio-frequency or rf or H_1 field). This method is called "magnetic resonance".

Optically pumped magnetometers which use alkali vapors were first suggested by Dehmelt (1957) and demonstrated by Bell and Bloom (1957). Two basic methods of monitoring the atomic resonance and thereby measuring the magnetic fields have been developed. One, used in M_z type of locked oscillator magnetometers, in which the resonance is detected by sweeping the field or frequency through resonance and monitoring the slow changes in pumping light intensity, Malnar (1961). The other method, used in M_x self-oscillating magnetometers, makes use of the radio-frequency modulation of the cross light beam which occurs at resonance. With the proper feedback this type may be turned into an oscillator whose frequency is proportional to the ambient magnetic field, Bloom (1962).

We have spent most of our research investigating optically pumped K (potassium) vapor magnetometer which operates as a self-oscillator. Self-oscillating magnetometers offer several important advantages over the locked oscillator type: 1) they are electronically simpler, requiring no modulation and resonance detection circuitry; 2) the absence of low frequency modulation makes the task of frequency measurement much easier; 3) they have very short response time, without limitations imposed on the rate of tracking; 4) they are self-starting, requiring no lengthy and complex sweeps to acquire lock; and 5) low frequency perturbations of the light intensity do not contribute to the magnetometer noise. The advantages 3) and 4) are two main reasons why the self oscillating magnetometer is considered the only practical embodiment to be used for ground search mode magnetometer. The self-oscillator's disadvantage of requiring an amplifier with precise and constant phase shift over the full measurement range is currently greatly alleviated by the availability of fast photodetectors and electronics. Although the locked oscillator has no polar dead zones, it has a larger equatorial dead zone than the self-oscillator. Consequently the total dead zone area is larger for the locked oscillator.

The configuration of the self oscillating type of optically pumped magnetometer is shown on Figure 1. The light of an electrodeless K lamp is filtered to pass only the D1 spectral line through the circular polarizer and the absorption cell. The component of the polarized light in the direction of the ambient field is responsible for the optical pumping. The optical pumping takes place in the absorption cell which contains K vapors and an inert buffer gas, and it results in a momentary alignment of the atomic angular momenta along the direction of the light beam. The atomic dipoles then precess about the ambient field at the Larmor precession rate, in the same sense but with random phase. A
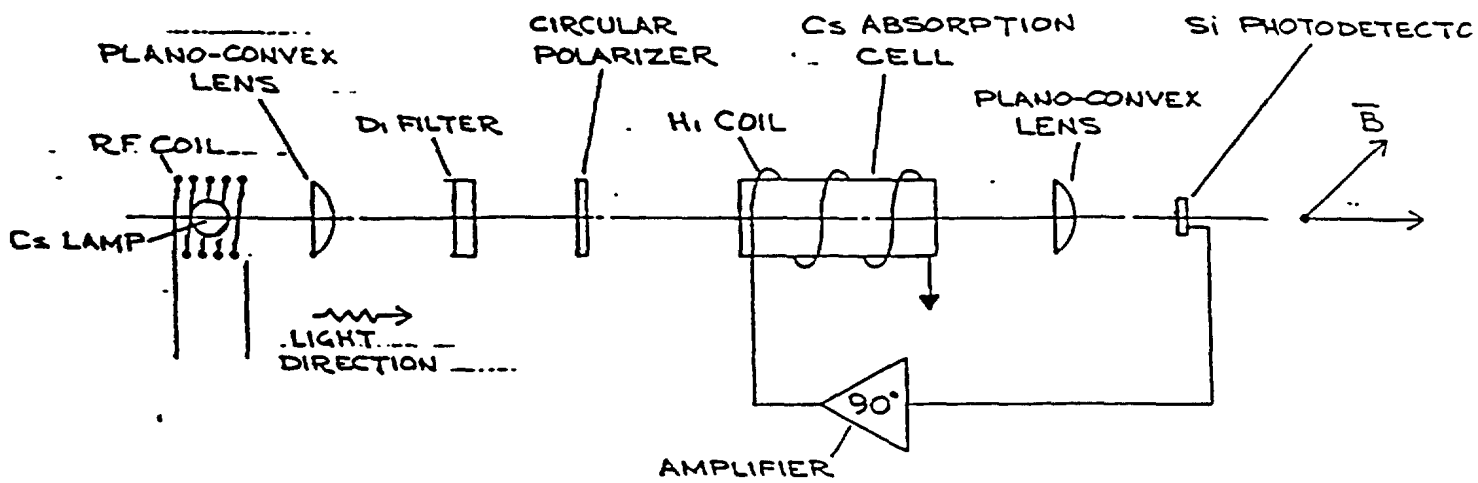
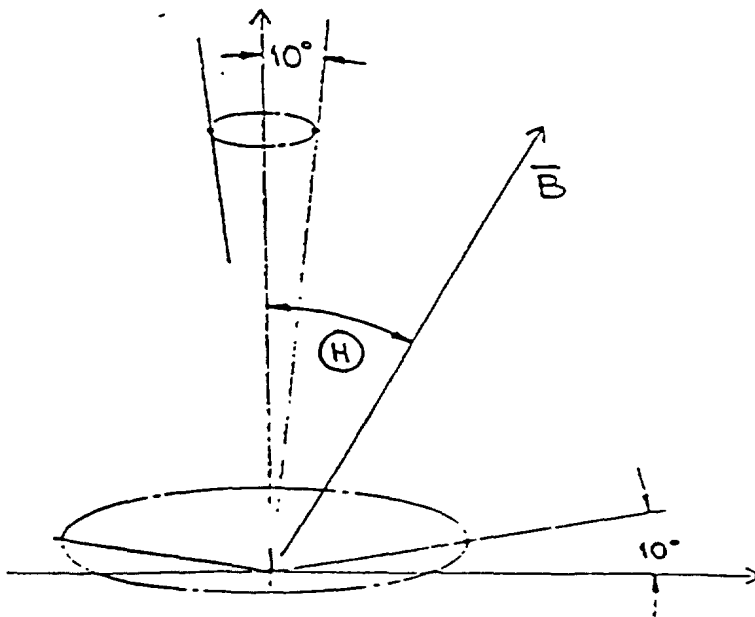Fig. 1

Single Cell Cesium Magnetometer

Fig. 2

Dead Zones of the Self-Oscillating Manetometer

magnetic field (H1 field) rotating about the ambient field at the Larmor frequency in the correct sense produces phase coherence of the precessing atomic magnetic moments. The precession of this net alignment causes a modulation of the light beam perpendicular to the magnetic field (the looking light) to occur at the precession rate, owing to the dependence of the optical absorption of the aligned sample upon its orientation with the direction of the light beam.

The optical modulation at the Larmor frequency is detected by a photodiode, amplified and fed back with the proper phase to supply the H1 field necessary to produce phase coherence. The system self-oscillates at the frequency determined by the Larmor precession of the atoms of K vapor in the ambient magnetic field. In case of potassium 39 with 4 separated, resonant line the magnetometer oscillates on the line which has largest amplitude. The magnitude of the ambient field is obtained by measuring the Larmor frequency, with a sensitivity limited by the measurement time available, the resolution of the measuring system and the Larmor signal noise.

2.2   Performance Characteristics

2.2.1   Heading Properties

The described magnetometer suffers, regardless which alkali vapor it uses to create magnetic resonance, from a so-called "hemisphere effect", whereby it only oscillates in one hemisphere. Careful control of the phase difference between the signal detected by the photodiode and the H1 field is required. The condition for self-oscillations at the peak of the resonance line is that the light modulation is ±90° out-of-phase with the H1 field. The opposite signs correspond to the opposite sense of rotation about the magnetic field direction. When the sense is arranged to be operating in the magnetic hemisphere for which a component of light intensity is along the positive field direction, it is possible to operate in the other hemisphere by reversing the sign of the 90° phase shift. Electronically, this simply means inverting the signal.

In the operating hemisphere there are polar and equatorial dead zones. Maximum signal occurs when the light beam is inclined at about 45° to the magnetic field vector, and reliable self-oscillations can be achieved within ±35° from the optimum position with some degradation of S/N ratio close to the dead zones. Dead zones, within which the signal amplitude drops rapidly and eventually no self-oscillation takes place, occur within ±15° of the field direction and its equator, Figure 2. The dead zones are properties of the optical pumping and the light modulation geometry. Close to the poles the effective intensity of the looking light and the effective H1 decrease rapidly, whereas close to the equator the effective intensity of the pumping light decreases rapidly. The dead zones can only be reduced or removed by an arrangement of two or three sensors which greatly complicates the design and increases the complexity of the magnetometer. The existence of the dead zones is not critical for the ground applications such as the ordnance detection.

2.2.2 Orientation Errors

All practical optically pumped magnetometers exhibit, to a greater or lesser degree, errors in reading which depend on the sensor orientation in relation to the ambient field vector. The magnitude of these errors can be appreciably reduced by different means, which include thoughtful design, compensation methods, and alignments. One of the main reasons for the orientation errors is that all alkali elements practically suitable for an optically pumped magnetometer exhibit few, closely spaced resonances, rather than one single and well defined one. Very often, such as in the cesium magnetometer presently produced by Scintrex, the eight resonant lines are so closely spaced that they overlap, resulting in a composite line of a magnetic resonance. (see pages 3-12 of our proposal). Their relative intensities depend on the optical pumping conditions, which vary with the position of the sensor with respect to the magnetic field. The resultant changes of this composite line lead to apparent changes of Larmor frequency and consequently the magnetometer reading. The main reason for investigating the potassium 39 magnetometer is that it has 4 resonant lines which are much farther apart in weak fields than these in cesium 133. In fact, for 50,000 nT ambient field intensity, the resonant lines are spaced 400 Hz apart in 39K, compared to 6.6 Hz in 133 Cs. In potassium the line spacing of many times their half width made us believe that a magnetometer based on potassium could be developed with greatly reduced orientation errors. It is convenient to specify and measure the orientation errors as a function of two angular orientation:

a) the inclination angle Θ defined as an angle between the sensors optical axis and the ambient magnetic field vector. This angle can be changed by "tumbling" the sensor. The errors associated with this angular change will be conveniently called "tumble errors".

b) the spin angle φ is defined by the projection of the ambient field vector on the ends of the sensor cylinder, with the respect to some arbitrary index. This angle is changed by rotating the sensor about its optical axis. The errors associated with this angular change will be conveniently called spin errors.

Figure 3 depicts the angles Θ and φ. The gimbal system built at Scintrex' low gradient magnetic test facility for orientation tests of optically pumped magnetometers allows remote change of the inclination and spin angles.

2.2.3 Resolution and Sensitivity

The value of the magnitude of the ambient magnetic field is obtained by measuring the Larmor frequency, which is, in the case of the split beam potassium magnetometer, nearly linearly related to the field, with a proportionality constant of approximately 7 Hz/nT.

One apparently simple and frequently used method of precision frequency measurement is to measure, with high time resolution, the average period over a pre-determined time interval and then to calculate the average frequency as the
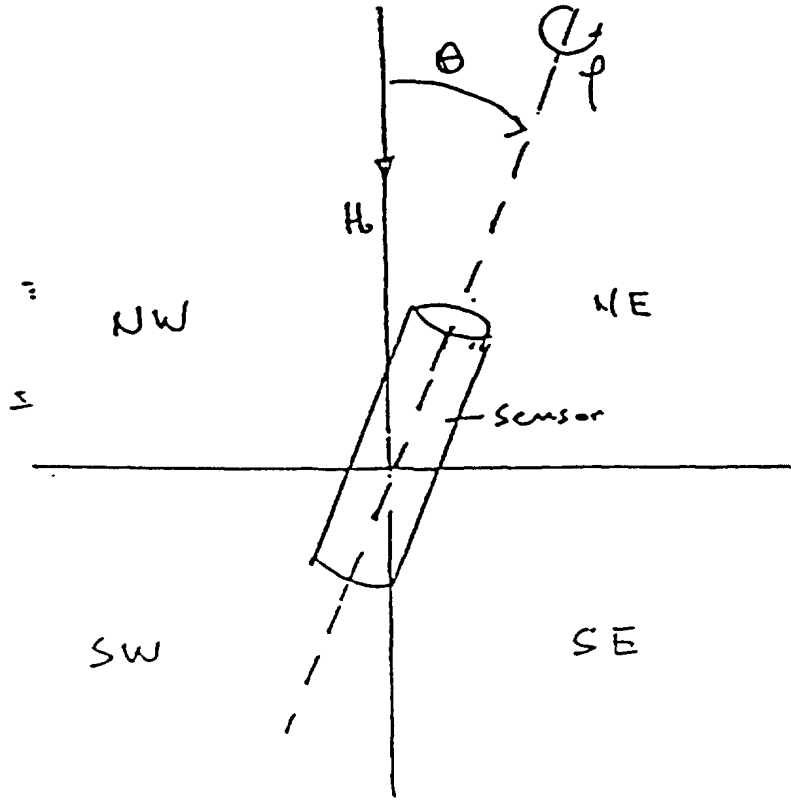
Fig. 3

Orientation Angles

inverse of the average period. If the field of up to 100,000 nT is to be determined with a resolution of 100 pT, 10 times per second, this requires the capability to measure time intervals with the precision of 100 ns, which is technically not a very demanding task.

The sensitivity of the optically pumped alkali magnetometers is much better then the required resolution of 100 pT and it is not a critical parameter in design of a ground search mode magnetometer.

3.0   ABSORPTION CELL DEVELOPMENT

The gas cell, otherwise known as a resonance or fluorescence cell, is a glass cylinder 25 mm in diameter and 25 mm long. Its ends are flat and it is fitted with optical windows, one of which has two small tips located near the edge. One of them contains deposit of metallic potassium, the second one indicates where the connection to the vacuum system was. In addition, a gas cell is filled with so called "buffer gas" at the pressure varying from few to few tens of Torrs. The purpose of a buffer gas is to keep optically oriented atoms in their quantum states as long as possible, by preventing disorientational collisions of atoms with a glass wall of a gas cell. The gases most commonly used for this purpose are argon, krypton and nitrogen. Although there are some general indications which gas and what pressure would provide good results, the final selection is still a matter of trial and error method. In the gas cell of an optically pumped potassium magnetometer, the magnetic resonance, frequency of which defines the measured magnetic field, takes place between Zeeman sublevels of the $4^2S_{\frac{1}{2}}$ F=2 ground state of potassium, which is shown in Figure 4.

The frequency of the transition between sublevel m_F and m_F+1 of the hyperfine state F=2 can be calculated from the Breit-Rabi formula and is given by

$$\nu = \frac{\gamma}{2\pi} H_0 - (2 \ m_F-1) \ \frac{\Gamma}{2\pi} \ (H_0)^2$$

where for 39_K

$$\frac{\gamma}{2\pi} = 700391 \ \frac{Hz}{gauss}$$

and

$$\frac{\Gamma}{2\pi} = 1065 \ \frac{Hz}{gauss}$$

So the ratio frequency spectrum (of the $4^2S_{\frac{1}{2}}$ F=2 state of potassium) will consist of four equidistant lines, separated by the frequency
$2 \times \frac{\Gamma}{2\pi} \ (H_0)^2$ Hertz

m_F

PEAK
NUMBER
(IN FIG. 7A)

1

2

3

4

2

1

0

-1
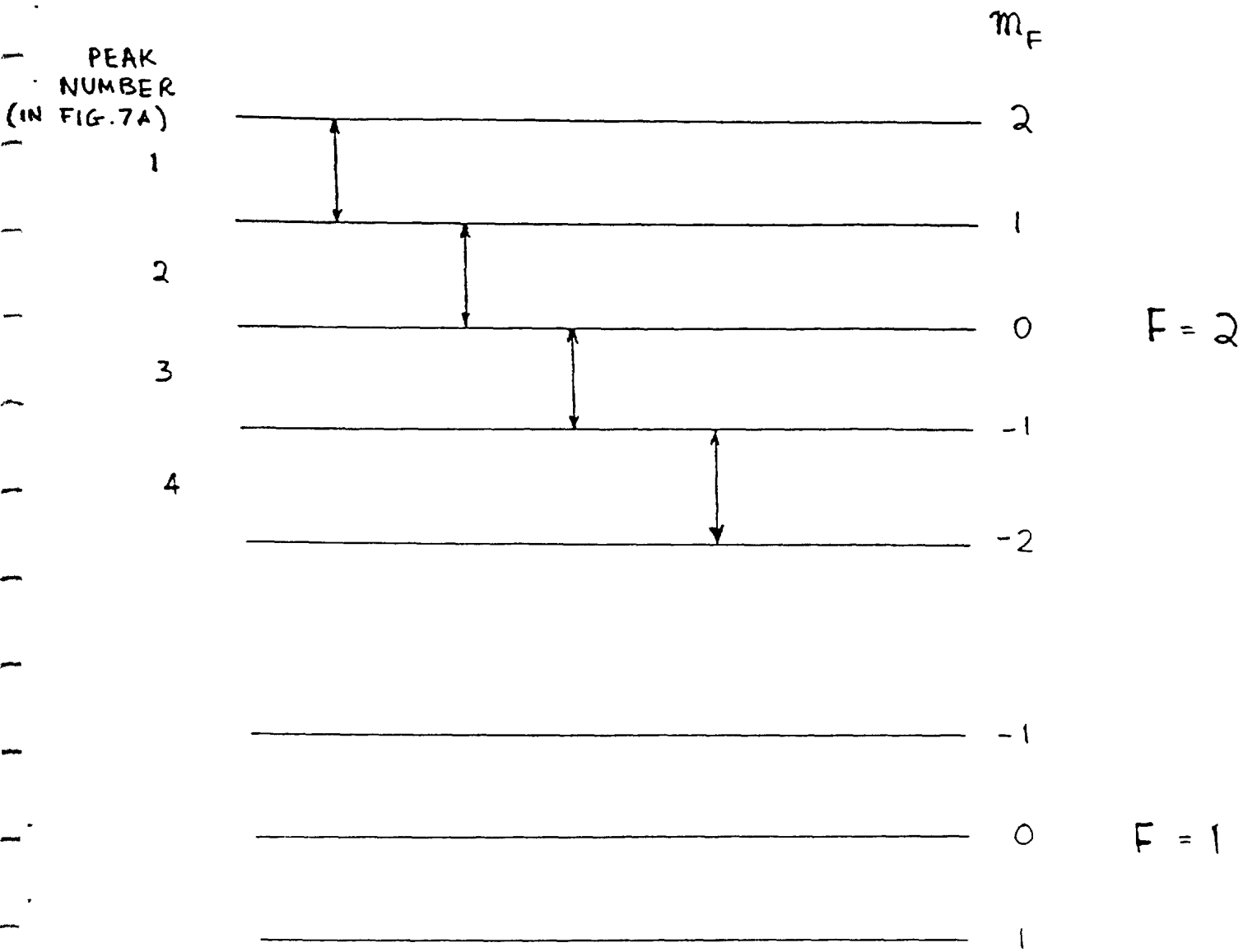
-2

$F = 2$

-1

0

1

$F = 1$

Figure 4

Zeeman Sublevels for 39K

The method of detection of transitions requires the prior establishment of a difference of population between them.

This is produced by an optical pumping with a circularly polarized light populating the sublevels with the highest value m_F. In the case of a polarized light, sublevel $m_F = 2$ is the most populated. This simply means that the most atoms are found to being in the $4^2S_{\frac{1}{2}}$ $F=2$ $m_F=2$ state. However, because of disorientational collisions, there are atoms in $F=2$, $m_F=1$ state, etc. Application of a radio frequency field H_1 (NOT TO BE CONFUSED WITH THE rf FIELD WHICH IS USED FOR LAMP EXCITATION!) induces transitions between Zeeman sublevels, resulting in change of transparency of the potassium vapor, which are registered by a photodiode. Such an rf spectrum is shown in Figure 5.

Potassium vapor was irradiated with the σ+ polarized D_1 line. Recording was taken at the magnetic field $H_0 = 56881$ nT while the radio-frequency field H_1 was 2.25 nT. The line width of a single resonance peak is about 24.5 nT.

The minimization of the line width of magnetic resonance is of utmost importance, as it is directly connected to two most important features of the magnetometer: its sensitivity and its orientation error performance as explained in paragraph 4. The line width of a magnetic resonance depends on several factors, the most important of which are:

1. Transverse relaxation time T_2.

2. Intensity of an RF field H_1.

3. Pressure of the buffer gas.

4. Intensity of the pumping light.

5. Gradients of an ambient field.

6. AC field of the power line.

Relaxation time, which describes how long oriented atoms remain in their state, can be controlled in the gas cell by two means:

1. Addition of the buffer gas to the cell or,

2. Coating of the cell walls with a special paraffin.

The drawback of the latter technique is, that its technologically complicated. It requires special cleaning of the cell walls (deactivation), distillation of a paraffin into the cell and distribution of a paraffin into a very thin, even layer covering the whole interior. On the other hand, the buffer gas at higher pressure, which is sufficient to maintain long relaxation time, significantly broadens the line width of the magnetic resonance, thus decreasing the sensitivity of a magnetometer.
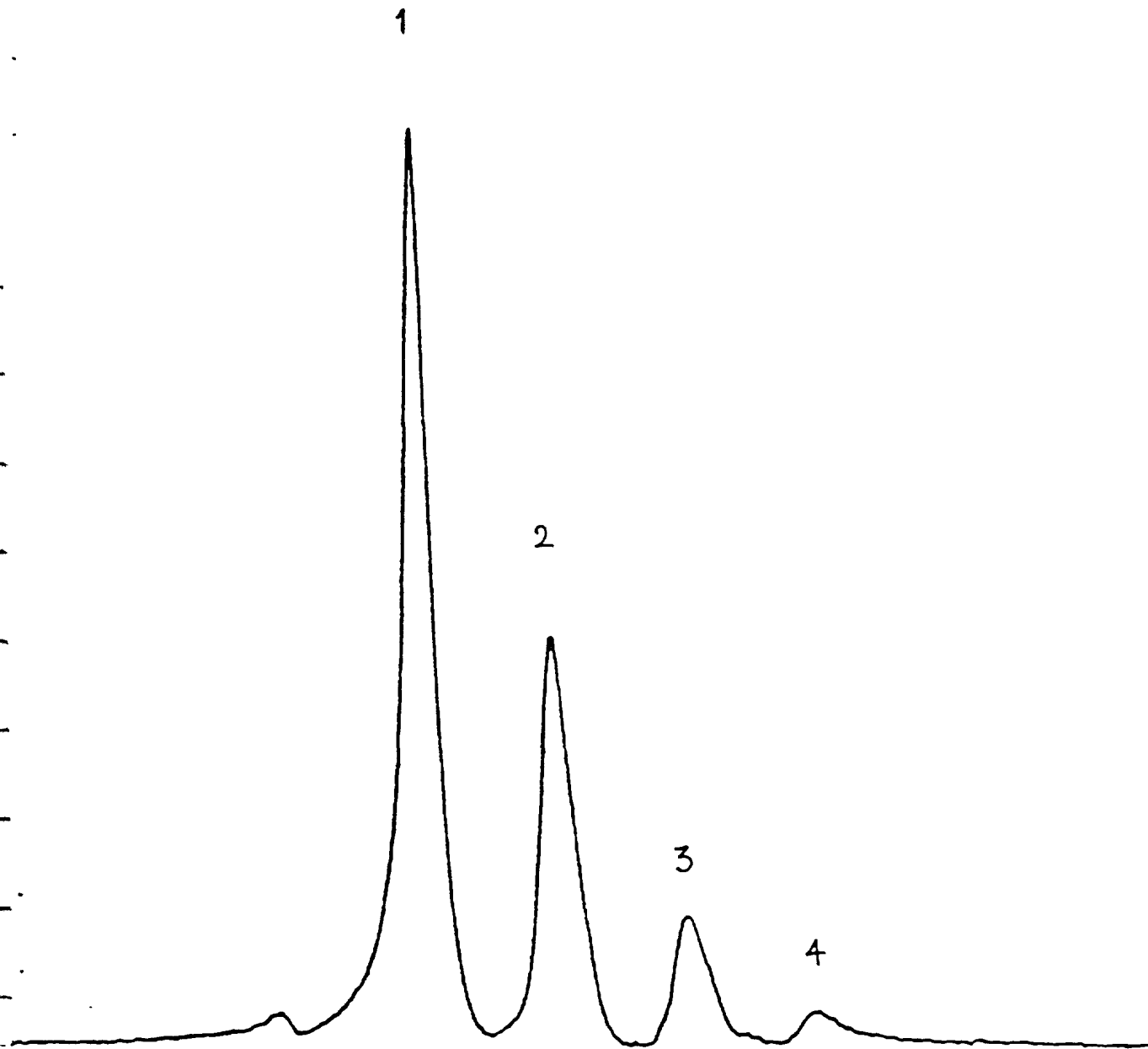
Radio-frequency spectrum of the $4 {}^2S_{\frac{1}{2}}$ F=2 state of ^{39}K taken at the magnetic field H_0 = 56881 . Peaks are separated by 688 Hz. The small peak on the left side of the spectrum arises from ^{41}K. Recording was taken in the shielded can. Sensor is oriented 40° off the direction of the magnetic field. Transitions marked in Figure 4 are indicated here.

Figure 5

A number of absorption cells has been manufactured with either nitrogen or argon as the buffer gas, and with different gas pressures. They were extensively tested at the Scintrex low magnetic gradient test site with help of instrumental set up described in Section 5.

Basically results indicate that: 1) Nitrogen works better than argon as a buffer gas (despite the fact that in the available literature the most common system is K-Ar, what prompted up to spend so much time on it).

2) The optimum pressure of a buffer gas for 2.5 cm long cell is around 50 Torr what is in good agreement with our theoretical prediction of about 40 Torr.

3) The longer cell (3.8 cm) works indeed far better than 2.5 cm long. 5 cm long cells happen to be too long for our present system – they possibly will be used later on.

4) The radiofrequency spectrum of the $4^2S_{\frac{1}{2}}$ ground state potassium is shown in Figure 6. Signal amplitude vs. pressure for N_2 cells is shown in Figure 7. Linewidth vs. pressure of N_2 is shown in Figure 8. As can be seen, a 35 Hz (5 nT) linewidth was obtained with a normal H_1 level drive. Further decrease of the H_1 drive resulted in the 25 Hz ($4\frac{1}{2}$ nT) linewidth, however, at the expense of signal to noise deterioration.

Our attempt to coat a cell with n-Tetracontane was unsuccessful. N-Tetracontane is a paraffin with melting point 80°C and at room temperature it is practically not soluble in any solvent. This poses considerable difficulties with its introduction into the cell, because of the small diameter of the capillary tube through which nitrogen, potassium and paraffin would be fed. At present there is no possibility to increase the capillary diameter without major changes in the gas cell design, what inevitably would require changes in the sensor design.

4.0   STUDY OF RESONANT LINES AND THEIR INTERACTIONS

4.1   Magnetic Resonance Line Study

As the basic advantage of an optically pumped potassium magnetometer is its potential ability to achieve orientation insensitivity by measuring the resonance of a single resonance line, the line study is of utmost importance.

The first effect which was studied was influence of the H_1 field intensity. It is a well known fact that the H_1 field affects the magnetic resonance. The first effect is its broadening followed by the change of its shape.

The slight shift of the resonance frequency caused by the H_1 field is known as the Bloch-Siegert effect. It is important, however, only in absolute measurements of the magnetic field, which are not very significant in the intended use of the search mode magnetometer.
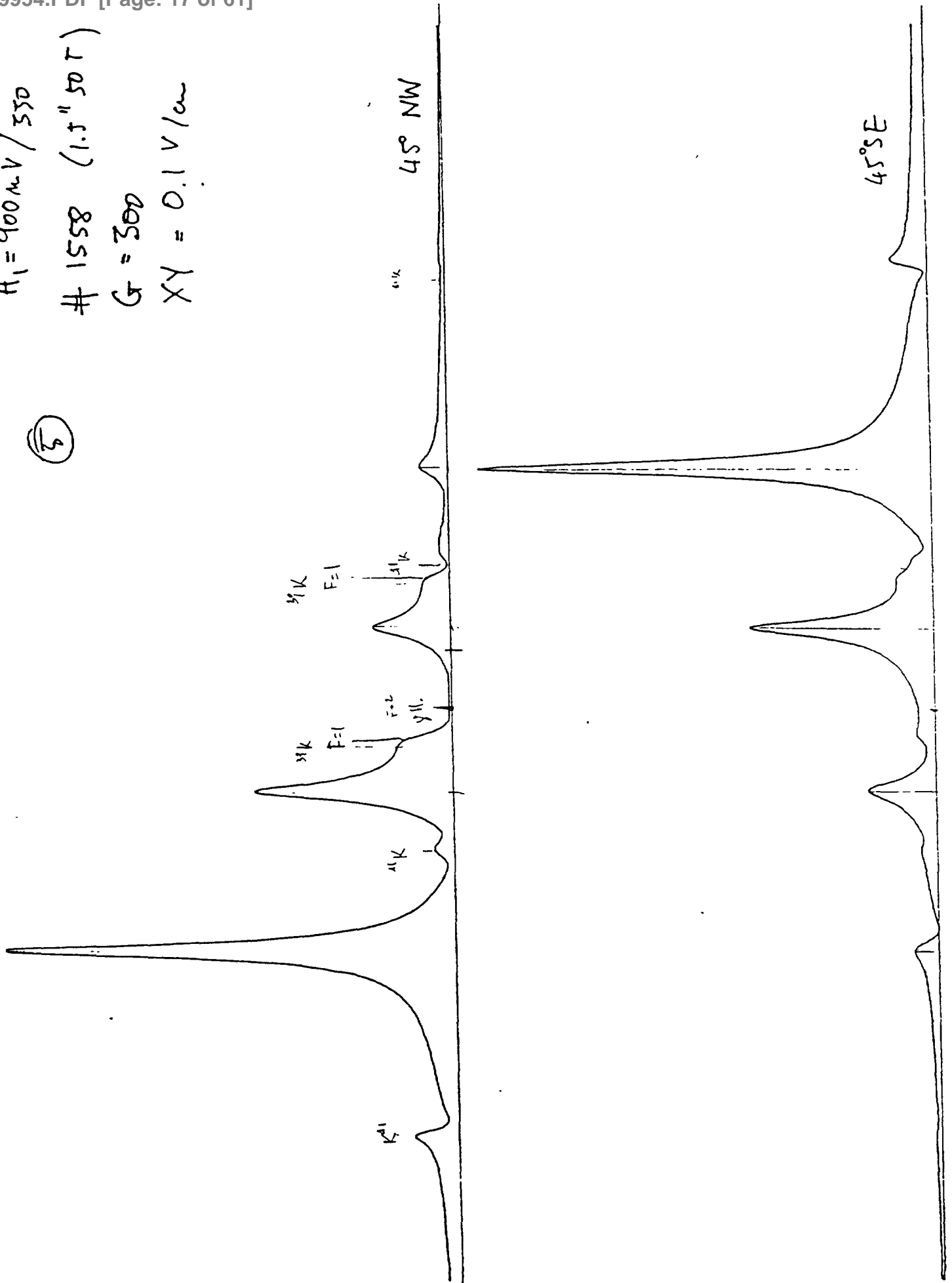
Fig. 6
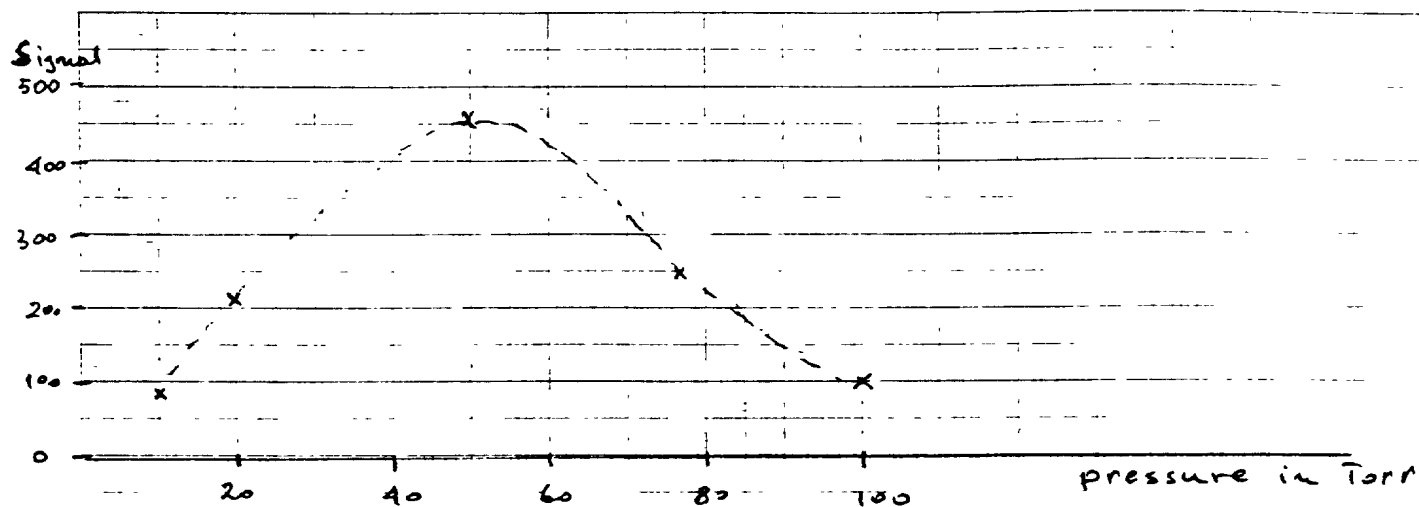
46 1513

Fig. 7

Signal Amplitude Versus
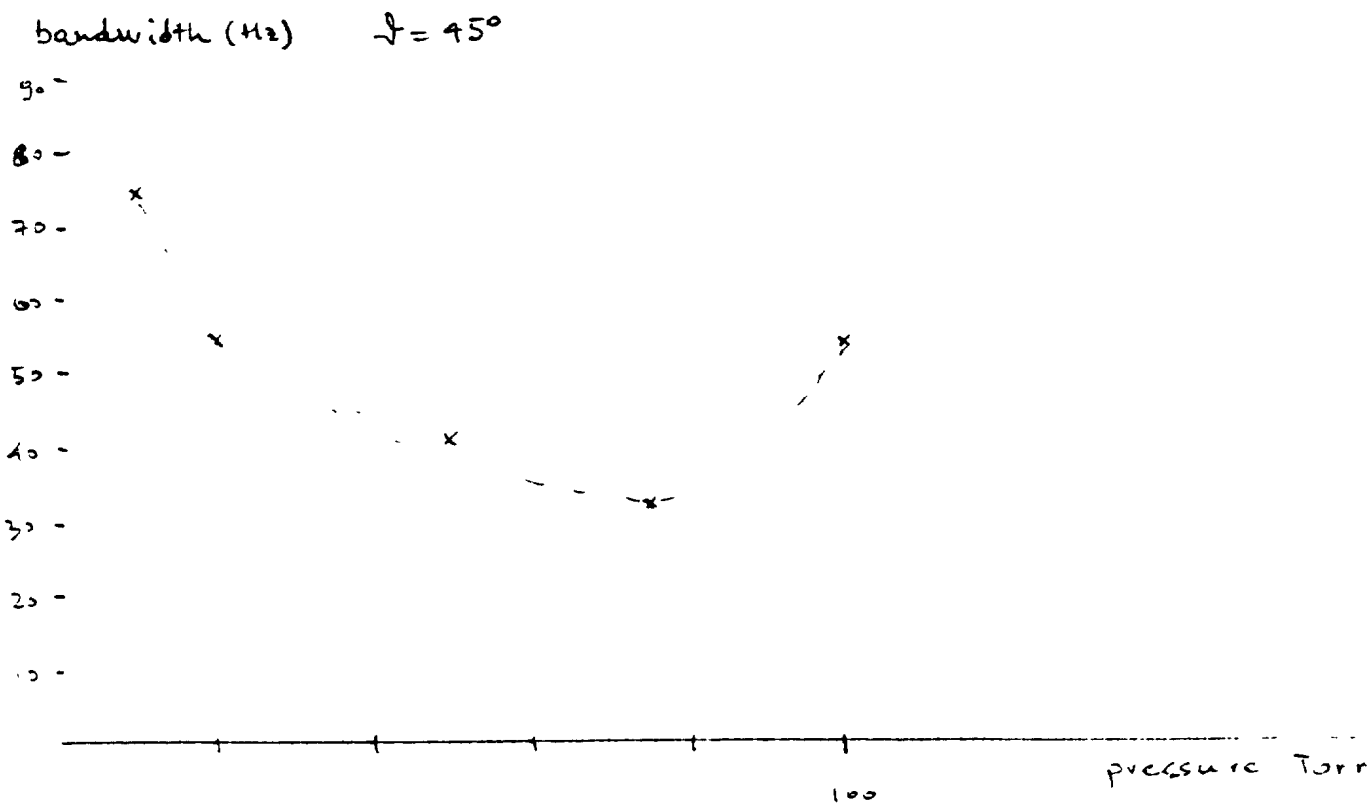Pressure for N2 Buffer Gas

bandwidth (Hz) $\vartheta = 45°$

Fig. 8

Linewidth Versus Pressure for N2 Buffer Gas

The width of the magnetic resonance is approximately given by an expression

$$W_L = \frac{2\,(1+(\gamma H_1)^2 T_1 T_2)^{\frac{1}{2}}}{T_2}$$

where

γ = gyromagnetic ratio of potassium
T_2 = is the transversal relaxation time
T_1 = longitudinal time constant

At the very low H_1 field intensities $(\gamma H_1)^2 T_1 T_2 < 1$ and

$$W_L = \frac{2\pi}{T_2}$$

The effect was examined confirming the characteristics described above, but at H_1 levels much higher than used for normal operation.

The second effort which was investigated is the structure of the magnetic resonance as a function of the field direction. As it was indicated the ideal conditions for the optical pumping are when the circularly polarized pumping light propagates along the magnetic field and the H_1 field is perpendicular to it. This leads to the largest population differences between the Zeeman states, resulting in the largest intensity differences between components of the rf spectrum. Creating and maintaining the intensity difference (making one line predominant) is a must for the self oscillating magnetometer described in Section 2. If two or more lines are of the similar amplitude, the magnetometer will oscillate at two or more different frequencies, making it far more difficult to measure the magnetic field. The change of the direction of the magnetic field with respect to the pumping beam has two effects on this structure:

1. Only a part of the light is used for optical pumping. This leads to the decrease of the magnitude of the resonances.

2. The polarization of light can be decomposed into three basic components σ^+, σ^-, and π, and in the case when a light beam makes an angle ϑ to a magnetic field, their intensities are given by:

$$I(\sigma^+) = \frac{I_0}{4}\,(1 + \cos\vartheta)^2$$

$$I(\pi^-) = \frac{I_0}{4}\,(1 - \cos\vartheta)^2$$

$$I(\sigma^-) = \frac{I_0}{2}\,(1 - \cos^2\vartheta)$$

Only the $I(\sigma^+)$ component is used for the pumping. The $I(\pi)$ and particularly $I(\sigma^-)$ components depump the system, destroying the achieved degree of orientation. This effect, being of extreme importance for a proper operation and the orientation error free operation of a magnetometer, was a subject of detailed theoretical and experimental studies. Four examples of experimental runs are shown in Figure 9a,b,c and d. The first corresponds to the position of a sensor 30° to the magnetic field, the next 60°, 75° and 80°. The most striking is the run shown in Figure 9d and the lowest frequency component is no longer the highest.

The spectral responses of an optically pumped single beam K-mag system have been measured in a gradient free environment. The amplitudes of the peaks corresponding to four dominant single level transitions of ^{39}K have been measured for several cells filled with nitrogen buffer gas. These amplitudes change with change of Θ, the angle between the optical axis and the direction of the ambient field. Typical variations of the normalized amplitude of the first dominant peak, and of the ratio $r_1 = A_2/A_1$ of the first and second peak amplitudes vs. the angular deviation from the polar dead zones are shown in Figure 10. As it may be seen, the A_1 amplitude varies over the range of 5:1, but even more critical is the amplitude ratio, r_1, which displays a variation from .1 to .8 over the desired operating range of orientations (15 to 75 deg.). The amplitude ratios $r_2 = A_3/A_3$ and $r_3 = A_4/A_3$ show similar variations as r_1, but are numerically somewhat smaller. The line width of the spectral peaks changes with the orientation as well.

4.2   Analytical Determination of Line Interaction

The basic issue in the design of an optically pumped magnetometer is the phase relation of an H_1 field to the optical signal received on the photodiode. The theoretical analysis of the system predicts the $\pi/2$ phase shift between the H_1 drive and optical signal in the case of σ^+ pumping when the system is in the resonance. This $\pi/2$ (or 90°) phase shift must be maintained over the whole operational range of a magnetometer, i.e. for all the frequencies. The resonance phenomena encountered in an optically pumped alkali vapor magnetometer may be represented by a model consisting of multiple single tuned resonant circuits. An analysis based on similar principles has been performed by Yabuzaki (74) for a Cs magnetometer in an attempt to theoretically predict the shifts of the resonant frequency for the spectral lines which are overlapping, and to calculate the degree of compensation of these shifts in a single beam Cs magnetometer.

A magnetometer employing a single resonant line for determination of the ambient magnetic field has to measure either the frequency of the zero crossing of the phase, or the frequency of the maximum amplitude for the calculation of the field. The resonant lines are relatively closely spaced: 700 Hz or 100 gammas in the ambient field of 60,000 and only 77 Hz to 11 gammas in the ambient field of 20,000 gammas. As such a close spacing the existence of adjacent peaks induces the frequency (field) shift f_p in the position of the frequency of phase zero crossing, and the shift f_a in the position of the maximum amplitude position. The magnitude of these shifts varies with the change of the amplitude
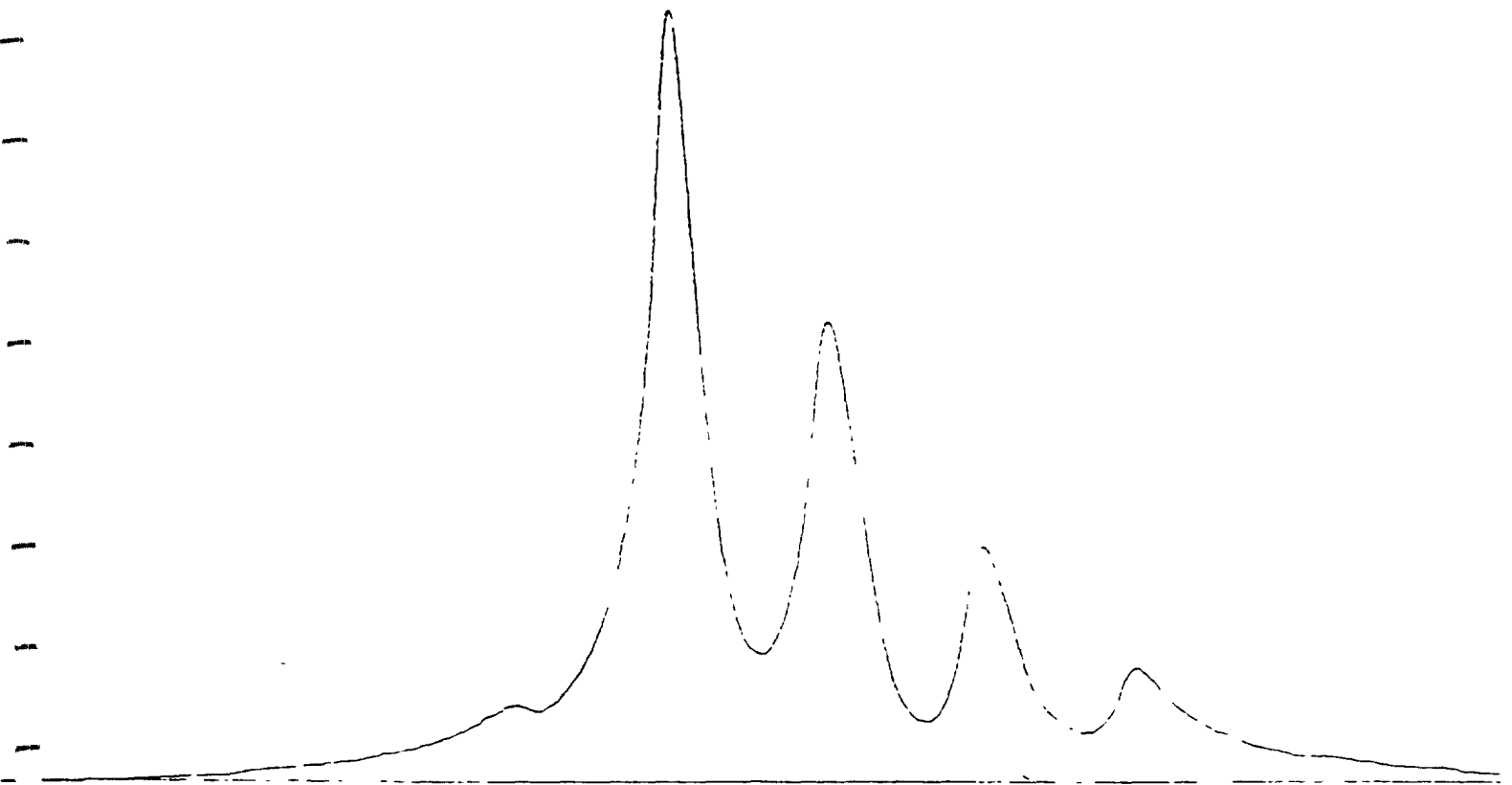
Fisgure 9a

Radio-frequency spectrum of the $4^2S_{\frac{1}{2}}$ F=2 state of potassium sensor at 30° to the magnetic field.
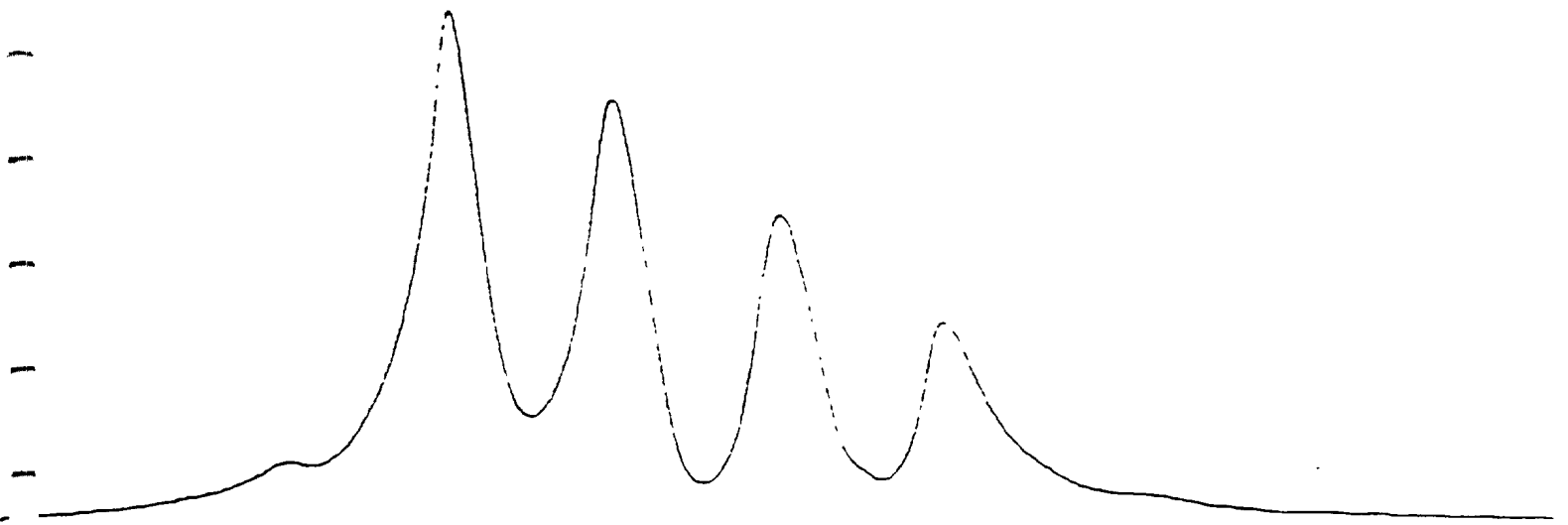
Figure 9b

Sensor 60° to the magnetic field
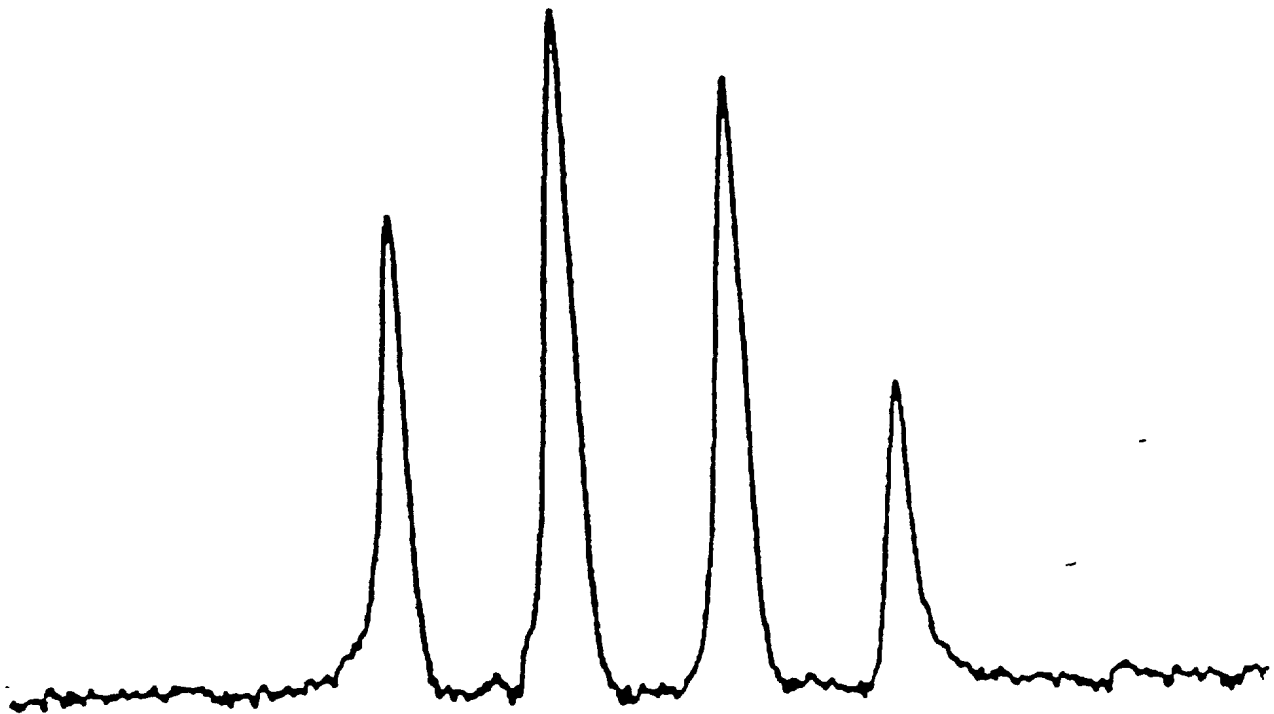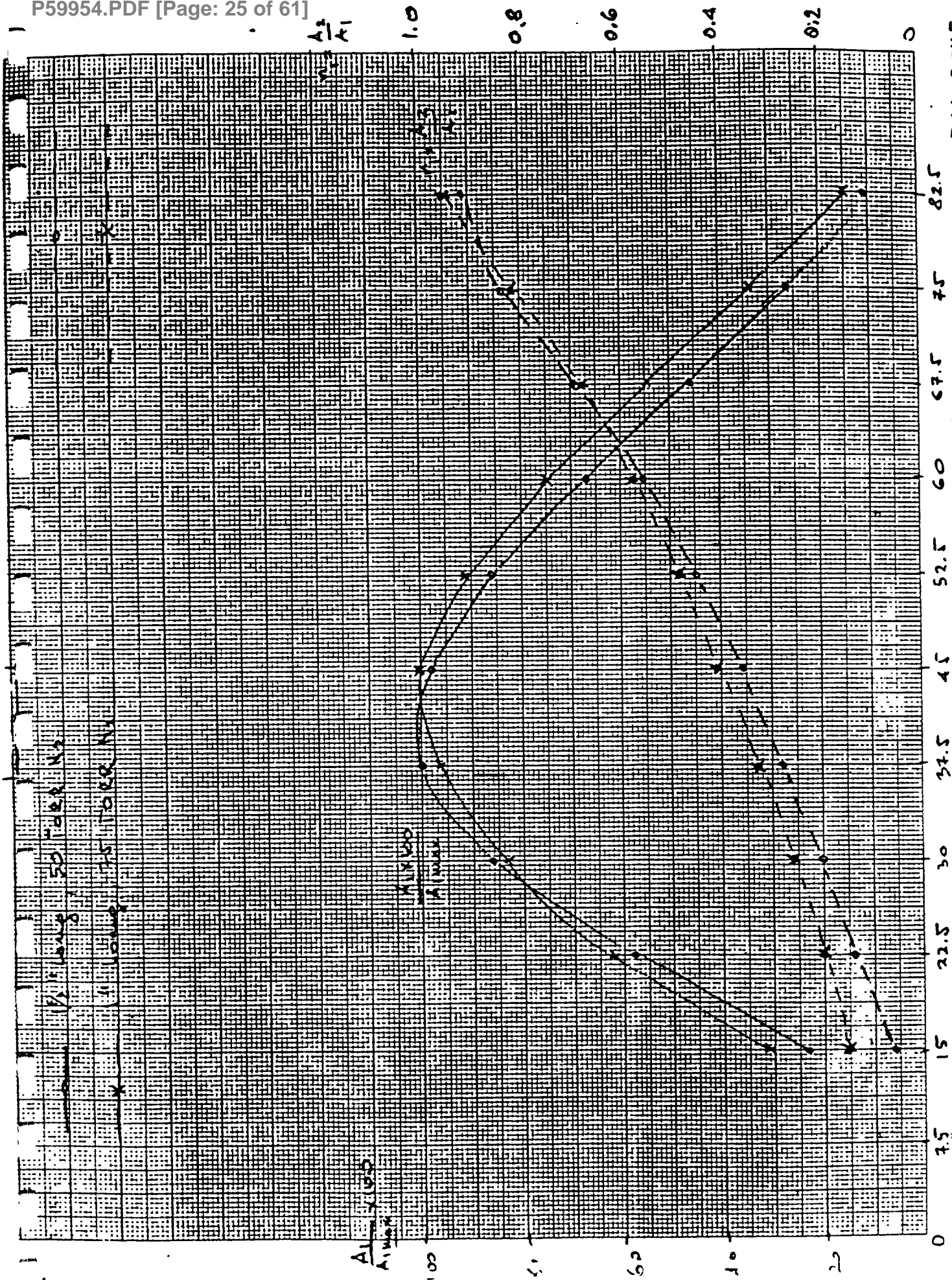
Figure 9c

Sensor 75° to the magnetic field

Figure 9d

Sensor 80° to the magnetic field. There is a change of scale of Y axis between 9c and 9d.

Fig. 10   46 1513

Angular Dependence of A1 and A2/A1

and the line width of the adjacent spectral peaks. The peak amplitudes and the line widths themselves are functions of the magnetometer orientation. The result of this interdependence is an orientation dependent error (heading error) which corrupts the instrument readings. The determination of the magnitude of the heading errors and the factors which influence them is of great importance. An analytical as well as a numerical solution are presented in this and next section.

Initially a simplified model was analyzed consisting of only two resonant peaks which have the amplitude ratio $r = A_2/A_1$ are are separated by s (normalized separation $s_n = s/0.5f_B$ is used). Both peaks have the same 3db line width f_B.

Equation (1) relates the normalized shift in the position of the phase zero crossing $f_{pn} = f_p/0.5f_B$ with the parameters r and sn.

$$(r+1) \ r_{pn}^3 + s_n \ (r+2) \ f_{pn}^2 + (s_n^2 + r + 1) \ f_{pn} + s_n \ r = 0 \tag{1}$$

For separations which are large compared with the line width, $s_n > 6$, the higher order terms may be neglected, resulting in a simple expression for the shift $f_p = f_r - f_p$ of the phase zero crossing position f_p, from the resonant frequency f_r, which would exist in absence of the disturbing peak A_2.

$$f_p = -r(f_B)^2/4s \tag{2}$$

The analytical solution for the determination of the position of the maximum amplitude of the peak A_1 in the presence of one disturbing peak A_2 (same conditions as used in he phase shift study) proved to be even more complicated. Only the solution for large s_n could be easily obtained. The expression for the shift of the maximum amplitude position $f_a = f_r - f_a$ is

$$f_a = r \ (f_B)^2/4s \tag{3}$$

which is opposite in sign from expression (2) but equal in amplitude.

4.3   Numerical Line Interaction Determination

It became obvious that only very simple cases of line interaction could be solved analytically. The numerical solution could provide much needed answers for relatively close line spacing, for which the analytical solution leads to unsolvable equations. The numerical solution was obtained for the case of four resonant peaks which have the same line width f_B and the same adjacent peak amplitude ratio $r = A_2/A_1 = A_3/A_2 = A_4/A_3$, and which are separated by s (which is ambient field dependent).

The results of this numerical analysis are presented in tabular form. Table I, II, and III list the phase zero crossing position shift and the maximum amplitude position shift of the dominant peak, for the line widths of 10, 5 and 2.5 gammas, as the result of interaction with the lines which have amplitude ratios in the range of 0 to 1, an equal line width f_B, and the line separation which would be encountered in fields in the range of 20k to 60k gammas.

Δfp=shift of zero phase position (gammas)
Δfa=shift of maximum amplitude position (gammas)
s=line separation (gammas)
r=A2/A1=A3/A2=A4/A3=amplitude ratio

fB=10=line width (gammas) TABLE I

r	s=100γ H=60,000γ		s=69γ H=50,000γ		s=44γ H=40,000		s=25γ H=30,000γ		s=11γ H=20,000γ	
	$\Delta fp(\gamma)$	$\Delta fa(\gamma)$	$\Delta fp(\gamma)$	$\Delta fa( )$	$\Delta fp(\gamma)$	$\Delta fa(\gamma)$	$\Delta fp(\gamma)$	$\Delta fa(\gamma)$	$\Delta fp(\gamma)$	$\Delta fa(\gamma)$
0.000	0.000	0.000	0.000	0.000	0.000	0.000	0.000	0.000	0.000	0.000
0.200	0.055	-0.055	0.080	-0.075	0.125	-0.120	0.213	-0.190	0.440	-0.255
0.400	0.125	-0.123	0.182	-0.178	0.284	-0.270	0.498	-0.424	0.800	-0.500
0.600	0.213	-0.210	0.310	-0.300	0.489	-0.445	0.876	-0.675	2.300	-0.770
0.800	0.325	-0.318	0.470	-0.450	0.753	-0.660	1.416	-0.960	10.790	-1.000
1.000	0.463	-0.443	0.680	-0.625	1.130	-0.915	2.325	-1.260	12.750	-1.173

fB=5=line width (gammas) TABLE II

r	s=100γ H=60,000γ		s=69γ H=50,000γ		s=44γ H=40,000γ		s=25γ H=30,000γ		s=11γ H=20,000γ	
	$\Delta fp(\gamma)$	$\Delta fa(\gamma)$	$\Delta fp(\gamma)$	$\Delta fa(\gamma)$	$\Delta fp(\gamma)$	$\Delta fa(\gamma)$	$\Delta fp(\gamma)$	$\Delta fa(\gamma)$	$\Delta fp(\gamma)$	$\Delta fa(\gamma)$
0.000	0.000	0.000	0.000	0.000	0.000	0.000	0.000	0.000	0.000	0.000
0.200	0.015	-0.015	0.020	-0.020	0.031	-0.030	0.055	-0.053	0.123	-0.105
0.400	0.030	-0.030	0.045	-0.045	0.071	-0.070	0.125	-0.120	0.283	-0.225
0.600	0.055	-0.055	0.078	-0.075	0.121	-0.120	0.215	-0.200	0.520	-0.360
0.800	0.080	-0.080	0.117	-0.115	0.185	-0.180	0.330	-0.295	0.830	-0.508
1.000	0.115	-0.115	0.165	-0.163	0.250	-0.240	0.479	-0.410	1.538	-0.657

fB=2.5=line width (gammas) TABLE III

r	s=100γ H=60,000γ		s=69γ H=50,000γ		s=44γ H=40,000γ		s=25γ H=30,000γ		s=11γ H=20,000γ	
	$\Delta fp(\gamma)$	$\Delta fa(\gamma)$	$\Delta fp(\gamma)$	$\Delta fa(\gamma)$	$\Delta fp(\gamma)$	$\Delta fa(\gamma)$	$\Delta fp(\gamma)$	$\Delta fa(\gamma)$	$\Delta fp(\gamma)$	$\Delta fa(\gamma)$
0.0000	0.0000	0.0000	0.0000	0.0000	0.0000	0.0000	0.0000	0.0000	0.0000	0.0000
0.2000	0.0035	-0.0035	0.0050	-0.0050	0.0078	-0.0077	0.0140	-0.0138	0.0313	-0.0300
0.4000	0.0078	-0.0078	0.0115	-0.0114	0.0177	-0.0177	0.0313	-0.0310	0.0711	-0.0670
0.6000	0.0133	-0.0132	0.0192	-0.0192	0.0303	-0.0303	0.0533	-0.0520	0.1221	-0.1115
0.8000	0.0202	-0.0197	0.0295	-0.0295	0.0146	-0.0455	0.0811	-0.0790	0.1883	-0.1650
1.0000	0.0287	-0.0285	0.0415	-0.0413	0.0654	-0.0645	0.1158	-0.1110	0.2739	-0.2265

The tabulated numerical solutions for the shifts could be used in calculating the orientation sensitivity characteristics of the present magnetometer embodiment. It is worth noting that in reality the amplitude ratios are not equal: r_2, and r_3 are somewhat smaller than r_1. This should not affect the magnitude of the shifts greatly, as the influence of the second, i.e. nearest peak is the predominant one. Of the larger influence in assessing the interaction effects with the change of magnetometer orientation is the fact that the line width itself changes with the orientation, making the exact determination somewhat more elaborate.

The relationships expressed by equations (1) and (2) are easy to determine from the Tables, which increases the confidence in accuracy of both deductions. The importance of decreasing the line width as the most influential parameter due to its power of two contribution is very obvious.

5.0   MEASUREMENT SYSTEMS

Two basic system configurations were used to make the measurements required. Figure 11 is a block diagram of the "open loop" measurement system. This system measures the phase and amplitude of the optical absorption response as a function of the H_1 frequency. The information can be recorded as amplitude vs. frequency in rectangular coordinates or as a locus of amplitude and phase in polar coordinates. The graphical data obtained is used to determine the effect of H_1 amplitude, light level, buffer gas pressure, and optical axis orientation relative to the Ho field etc. on the absorption line characteristics.

Figure 12 shows the "closed loop" or self oscillator measurement system. In this case the optical signal measured by the photodiode is amplified and phase shifted by the required amounts needed to fulfill the conditions for oscillation (0° phase shift and unity gain of the open loop system) and fed back to the H_1 coil. A sinusoidal output signal at a frequency determined by Ho is produced. Since this frequency is approximately twice the frequency produced by the cesium magnetometer for the same Ho, it is convenient to divide this frequency by two and mix it with the output of a cesium magnetometer to obtain:

$$\Delta f = \tfrac{1}{2} f_K - f_{Cs}$$

f_K = potassium magnetometer frequency

f_{Cs} = cesium magnetometer oscillator frequency

This difference frequency Δf is, to a first approximation, independent of changes in H_o, because it represents a gradiometer type of measurement. When the earth's magnetic field is used as H_o, the small fluctuations in field intensity have negligible effect on Δf because:

$$\Delta f \ll \tfrac{1}{2} f_K$$

The difference frequency Δf is counted, displayed and recorded to a useable resolution of 0.1 Hz.
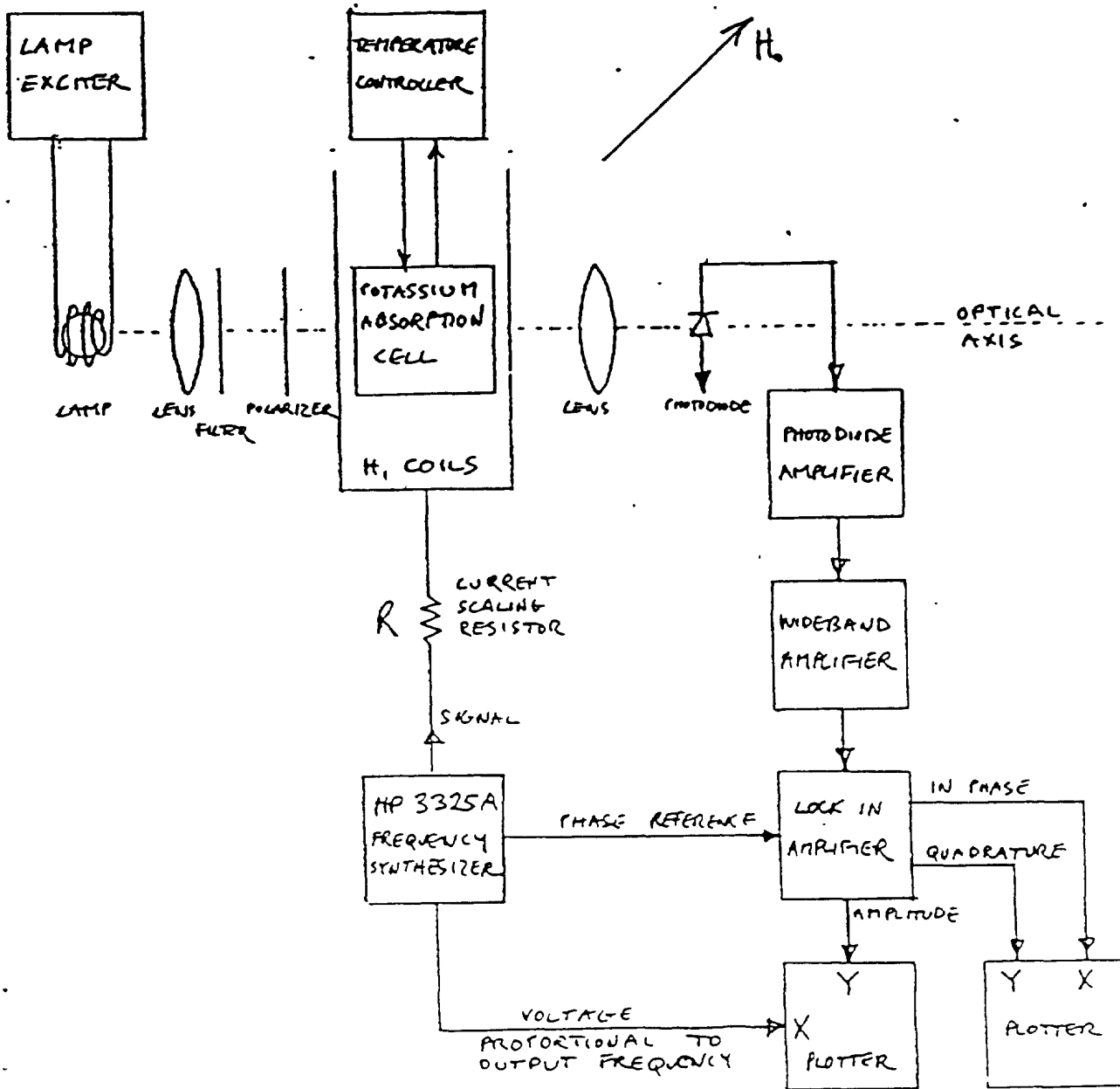
Figure 11

Open Loop Pressurant Line Measurement System

LAMP EXCITER

TEMPERATURE CONTROLLER

H_0

POTASSIUM ABSORPTION CELL

OPTICAL AXIS

LAMP

LENS

FILTER

POLARIZER

LENS

PHOTODIODE

PHOTODIODE AMPLIFIER

H_1 COILS

WIDEBAND AMPLIFIER

R — CURRENT SCALING RESISTOR

PHASE SHIFTER

AUTOMATIC GAIN CONTROL

FEEDBACK

H_0

BAND PASS FILTER

f_K

CESIUM REFERENCE MAGNETOMETER

f_{Cs}

FREQUENCY DIVIDER AND MIXER

Δf

FREQUENCY COUNTER

$\Delta f = \frac{1}{2} f_K - f_{Cs}$
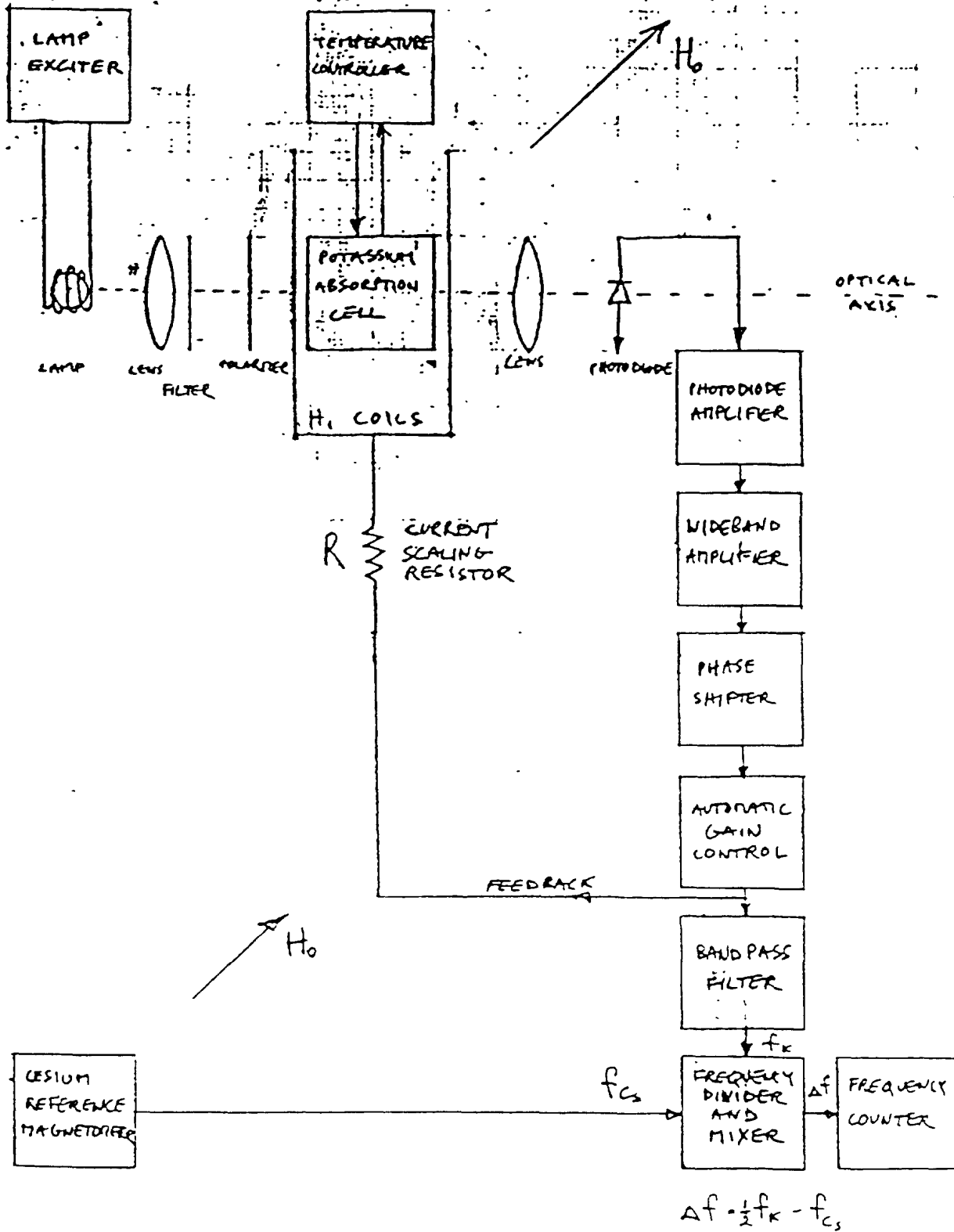
Figure 12

Closed Loop, Self Oscillaton Measurement System

This system is used mainly for conducting orientation measurements. These measurements were conducted at the Scintrex test facility which is located in a low gradient, low noise area. The potassium magnetometer sensor is installed in a gimbal system which allows the sensor to be positioned at a desired tumble or spin angle.

The cesium magnetometer is mounted in a fixed position approximately 15 meters from the potassium sensor and provides the reference frequency f_{Cs} proportional to Ho.

A spin test is conducted by fixing the tumble angle Θ and plotting Δf as a function of spin angle φ.

A tumble test is conducted by fixing the spin angle φ and plotting Δf as a function of the tumble angle Θ.

Change of Δf as a function of Θ and φ is known as orientation error.

5.1   Electronic Circuits

Most of the electronic subsystems shown in the block diagrams of Figure 11 and 12 were placed in separate plug-in modules and installed in a 19" equipment rack. This arrangement was chosen so that system changes could be implemented quickly and easily. A ±15 Volt power supply was used throughout. The major building blocks are described below.

5.1.1   Photodiode (Larmor) Amplifier

This consists of a wideband, low noise, preamplifier designed to convert the photodiode current signal to an output voltage signal. The frequency response to an optical input signal is from DC to approximately 1 MHz.

5.1.2   Wideband Amplifier

The amplifier has variable voltage gain from 3 to 1000 frequency response from 1 KHz to 5 MHz. This wide gain range allows a large range of photodiode signal amplitudes to be accommodated.

5.1.3   Lock In Amplifier

The lock in amplifier uses synchronous detectors and low pass filters to convert an AC signal to DC and greatly reduce noise levels. The outputs provided are in-phase and quadrature components of the input signal relative to a phase reference signal and amplitude of the input signal.

5.1.4   Automatic Gain Control (AGC)

This is a control system that maintains a constant output voltage for any input voltage within a certain range. It is designed to operate with negligible phase shift between the output and input signals. The AGC is used in the self oscillator system to maintain open loop gain of unity.

5.1.5   Phase Shifter

This unit can provide any desired phase shift from 0 to 360°. This permits easy adjustment of open loop phase shift to 0° as is required for oscillation to occur.

5.1.6   Bandpass Filter

This filter is used to improve the signal to noise ratio of the oscillator output signal for the purpose of frequency counting or for signal amplitude measurement using an AC voltmeter.

5.1.7   Temperature Controller

The temperature controller is designed to maintain a constant absorption cell temperature of approximately 70°C. A thermistor temperature sensor controls the output of a 10 KHz power oscillator used to provide power to the load. The load consists of a bifilar very fine copper resistance wire winding potted in a cylinder placed around the absorption cell.

5.1.8   Frequency Divider and Mixer

This circuit divides the potassium self oscillator frequency by 2 and mixes it with the output of a cesium self oscillator magnetometer. The mixer output is low pass filtered and is at a frequency Δf.

$$\Delta f = \tfrac{1}{2}f_K - f_{Cs}$$

This is used for orientation testing as described above.

The M.E.P. Gradiometer system can also be used to compute Δf. The frequency divider and mixer was built because the M.E.P. was not always available for our use.

5.1.9   Lamp Exciter

The lamp exciter used for the potassium lamp consists of a 110 MHz R.F. oscillator driving a small coil enclosing the potassium lamp. The oscillator power level can be adjusted to set the desired light level.

A potassium lamp with a heated potassium reservoir was assembled and tested. The reservoir was held at a temperature of approximately 150°C and the potassium vapour was excited by an 110 MHz RF oscillator of the type used in the Scintrex cesium magnetometer. This technique produced D1 light output of sufficient intensity and short term stability for our experiments. However after several hours of operation the light output would begin to drop, probably due to migration of the potassium vapour from the discharge bulb through the interconnecting channel into the reservoir. It appears that adjustment of the length and diameter of the channel might solve this problem. For conducting the most experiments a potassium lamp similar in design to the existing cesium lamp.

14

6.0   DEVELOPMENT OF PROTOTYPE SIGNAL PROCESSOR

A bench prototype of Larmor signal processor has been built, programmed and tested. It was designed to comply with the requirements for microprocessor based electronic package of a portable search mode K-magnetometer (Phase II of the project) with following design goals:

1. Sensitivity, better or equal to 0.1 nT.

2. Measurement time of less than 0.1 second.

These goals have been achieved with in a single design depicted in block diagram in Figure 13.

The value of the magnitude of the ambient magnetic field is obtained by measuring the Larmor frequency, which is, in the case of potassium magnetometer, is nearly linearly related to the field, with a proportionality constant of approximately 7.0 Hz/nT.

The method used for precision frequency measurement is to measure, with high time resolution, the average period over a pre-determined time interval and then to calculate the average frequency as the inverse of the average period.

To achieve this an integer number a Larmor periods is counted in one counter, while 10 MHz clocks are counted during the same 0.1 second interval in the second counter. Microcomputer is programmed to calculate the average ambient field in 0.1 second interval based on the counts from these two counters. The magnetic field readings are output in ASCII format on RS-232 serial output.

The visual output is on 6 digital high brightness LED's. Different algorithms could be used to format the audio output via A/D converter and the speakers located in the headphone. The operator commands are accepted through a simple 3 key keyboard.

6 DIGIT LED 7 SEG

763 211

8 BUS

KEY BOARD

HEADPHONES

SP

SP DRIVER

VOLUME & PITCH CONTROL

AD

8K
1 x 5565
RAM

810
I/O
TIMER

16
2 x 2764
ROM

9600 BAUD

856
UART

RS 232
ASCII DATA
OUT

5 MHZ

800
CPU

8 MHZ

%

10 MHZ

÷2

20 MHZ
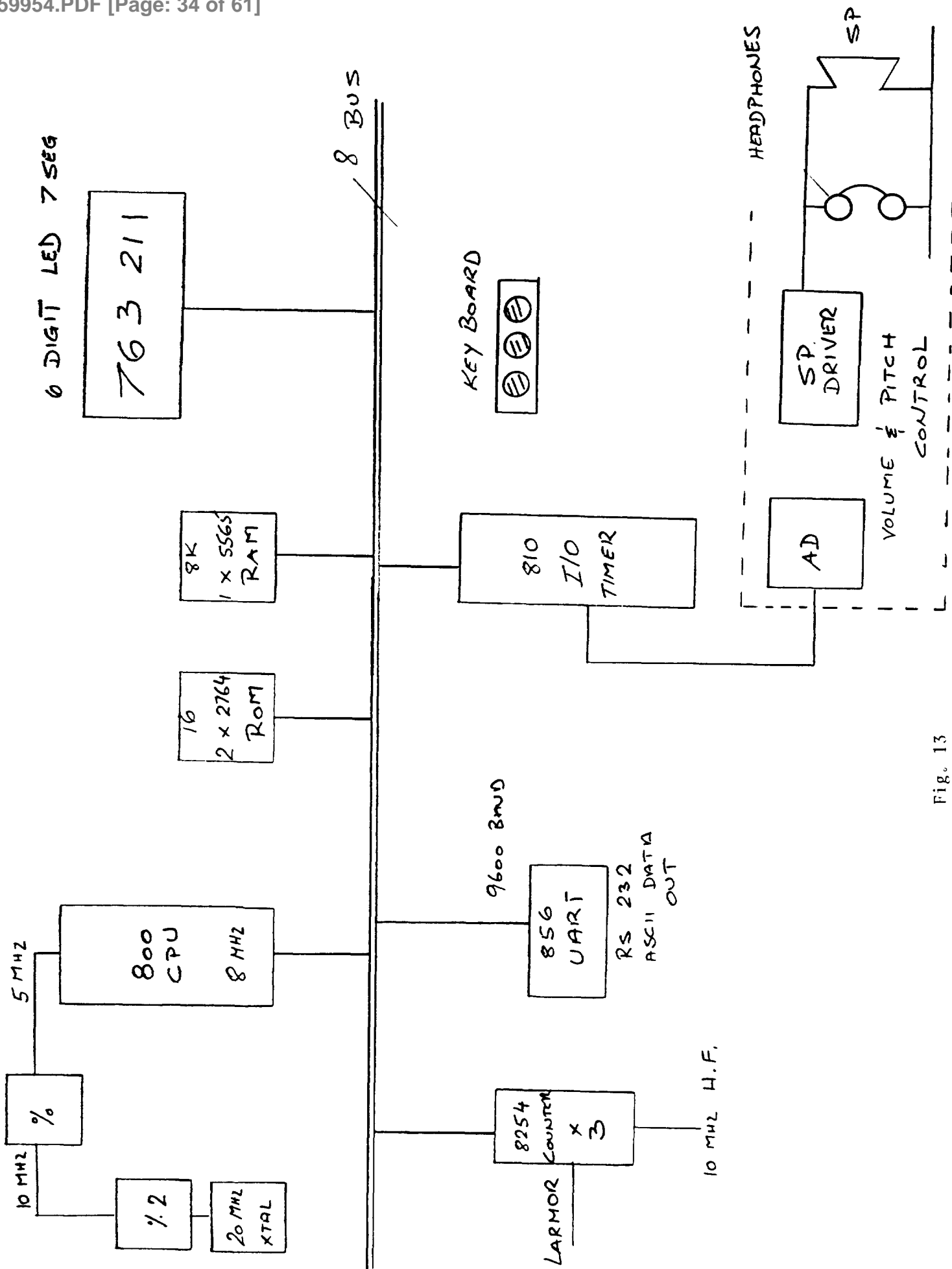XTAL

8254
COUNTER
x 3

LARMOR

10 MHZ H.F.

Fig. 13

Signal Processor for Search Mode Magnetometer

7.0   ORIENTATION ERROR DETERMINATION AND REDUCTION

A major advantage of K magnetometer was supposed to be its potential freedom of
orientation errors. As described in Section 4.2 of this report, the problem of
resonant line interaction and the resulting orientation error was recognized as
soon as the first spectra were obtained. This effect was theoretically
investigated, but the experimental verification, which was deemed necessary, was
still missing. As described in Section 5, the signal processing and orientation
error measurement electronics had to be greatly improved before we could close
the feedback loop and turn our experimental resonant line detection sensor into
a well operating single beam magnetometer (Larmor Oscillator), whose principle
of operation was described in Section 2. The experimental determination and
reduction of orientation error of this magnetometer turned out to be a major
undertaking. In the following four paragraphs of this section the tumble and
spin orientation measurements are described, and the potential sources of
orientation errors are listed and discussed.

7.1   Causes of Orientation Errors

A list and short description of the orientation errors of the self oscillating
single beam optically pumped potassium magnetometers is presented. Although
theoretically all of these causes are reported or known to affect the
orientation performance of optically pumped magnetometers, some of them are
insignificant, and some of them, it was thought, could be greatly reduced by
design. However, qualitative and quantitative understanding all of these
effects is required to design a K-mag with the low orientation sensitivity.

7.1.1   Resonant Line Interaction

The effect of the resonant line interaction is discussed in Section 4.2. This
effect should contribute less than 0.1 nT to the tumble error for operating
conditions of Ho = 60,000 nT, line width 5 nT. The effect becomes much more
significant at lower values of the ambient field Ho.

7.1.2   Resonant Frequency Perturbation by Light

In early optical pumping experiments it was discovered that in an optically
pumped vapour certain ground-state transition frequencies underwent a shift
which was proportional to the pumping light intensity. Quantum mechanical
analysis shows that the Zeeman light shift operator can be thought of as an
effective magnetic field which is directed either parallel or antiparallel to
the pumping light beam. Consequently, the light shift affects the Zeeman
frequencies in exactly the same way as we would a small magnetic field,
Mathur (68).

The resonant frequency variation due to the perturbation of the magnetic states by the pumping beam were investigated by Cohen-Tannoudji (62) and Schearer (61) for the case where the pumping beam and Ho field are aligned. Slocum (70) has experimentally investigated this effect for He magnetometer in the case the angle between the pumping beam and Ho changes. He has detected two types of shifts: a) an off-resonant light shift which is symetrical with respect to field reversal, i.e. it changes the polarity when the hemisphere of operation is changed. In the split beam Cs magnetometer in which one half effectively operates in nothern and one half in southern hemisphere the changes due to this effect cancel out. For that reason they were not noticed and they were largely unknown to the designers of the Cs split beam magnetometers, b) coherence narrowing shifts which are independent of the field reversal. The shifts due to the latter effect are smaller than the off-resonant light shifts. These shifts are proportional to the intensity of the $^+$, $^-$ and components of the exciting light which, as explained in Section 3 vary with inclination angle .

The experimental results reported in Section 7.4 prove unmistakably that the pumping light induced shifts pose the major problem in the design of low orientation error potassium magnetometer.

7.1.3 Resonant Frequency Perturbation by RF Fields

The effects of alternating electromagnetic fields in the rf region and higher than the resonance frequency were investigated by Yabuzaki (71). When its frequency ω is $\omega << h\gamma_0$ where h is its amplitude, the shift $\Delta\omega_0$ in the resonant frequency is given by:

$$\Delta\omega_0/\omega_0 = (\gamma_0 h \sin \Theta /2\omega)^2$$

100 MHz rf field of the lamp exciter would satisfy the above requirements, but to induce the observed effects of 0.5 nT it would have to be of amplitude $h = 10^{-4}T$. A current of more than 10A would have to flow through the lamp rf exciter coil to create such a large field inside the absorption cell. This effect is not likely to cause orientation error in our magnetometer.

7.1.4 Resonant Frequency Perturbation by H_1 Field

The theoretical investigations of the amplitude dependence of the resonant lines indicates a line broadening effect with the increase of H_1. However, the formula for the resonant signal does not indicate that the phase of the resonant signal is affected at all. The practical implication of this is that for a restricted range of H_1 the resonant frequency may not be dependent of H_1. We have experimentally observed the changes of the resonant amplitude shape induced by varying H_1 with kept constant and by varying O with H_1 kept constant. The attempts to measure these effects were inconclusive due to the presence of other larger orientation errors.

7.1.5 Effects Due to Alternating Fields

In presence of an alternating field of magnitude h, frequency ω and inclination α to the ambient field Ho the total field H_t is obtained from:

$$H_t = [(Ho + h\cos\alpha \cos\omega t)^2 + (h\sin\alpha \cos \omega t)^2]^{\frac{1}{2}}$$

Due to the nonlinear operations of squaring and taking the square root, the average value (DC component) of H_t differs from H_o. This effect was very likely responsible for different spin error characteristics with the heater turned ON or OFF. (See Section 7.3). In this case the source of AC fields was the heater current and the angle α between the alternating field and Ho was changing with the change of the spin angle ϕ. Careful tight twisting of the bifilar heater wiring reduced the effect greatly.

7.1.6   Errors Due to the Axis Misorientation

Bloom (62) has analyzed changes in resonant frequency due to the misorientation between the effective axis of the light beam and the axis of the resonant rf field H_1. If these axis are not exactly parallel to each other, then the axes spurious phase shift shows up as a spin error. The amplitude of this spin error is function of Θ : large errors occur only when Θ is small; however, under such conditions even a small misorientation angle can give rise to a large error. Special care is required in winding the rf coil and maintaining it fixed with respect to the absorption cell. Maintaining the well-defined axis of symetry of the optical system despite the broadness of the light source is equally important.

7.1.7   Errors Due to the Electronic Phase Shifts

In the vicinity of resonance, the amplitude of the signal is approximately constant, but the phase varies as $\Delta\psi = \dfrac{\pi/2}{f_B} \Delta f$, where f_B is the line width and Δf is the deviation from resonance. It is clear that any phase shift of the feed back loop different from 90° leads to a shift in frequency as change in the oscillation frequency has to compensate the spurious phase shift.

The line width changes with orientation angle Θ results in the change of the magnitude of this shift. The careful adjustment of the phase shift of the feed back loop reduced this effect. In addition, a narrow line width causes smaller frequency shift for a given spurious phase shift.

7.2   Tumble Orientation Tests

Our orientation error measurements started by varying the inclination angle Θ from 15° to 70° in all four hemispheres of operation with the spin angle kept constant (see Section 2.2.2 for definition of these angles). After the first set of tests, the problem of the amplitude dependent, phase shifts in the H_1 amplitude limiter (see Section 5.1.4) has been detected and eliminated by a better automatic gain control circuit. These phase shifts, which were dependent on the H_1 signal amplitude, caused the oscillation frequency to shift and contributed to the orientation errors.

Then, it has been discovered that the hybrid photodiode and preamplifier circuit, which was located not far from the absorption cell, has a magnetic signature because of DC current loops inside the hybrid. This was replaced by a separate photodiode and a newly designed preamplifier which is 1 m away from the sensor. The noise performance of this preamplifier is superior to the

previously used hybrid, which increases the sensitivity of the orientation error measurement. Some tests were conducted to detect whether change of magnitude of H_1 field affects the orientation errors, but they were, so far, inconclusive.

The measured orientation errors of about 0.5 nT were much larger than the predicted line interaction errors, which for the ambient field at 60,000 nT and the line width of 5 nT should not exceed 0.1 nT according to the error model studies (See Section 4.3). An extensive search through the available literature on optically pumped magnetometers was then undertaken in order to gain more understanding of the various factors which may contribute to the orientation errors. The description of different orientation error causes was given in Section 7.1 of this section.

The errors induced by the change of the intensity of the pumping light were experimentally detected. Their magnitude was large enough to warrant further investigation. At the same time a spin test was conducted which revealed large errors, see Figure 14. It can be seen that the magnitude of the tumble errors (the difference between the two curves for a constant θ) depends to a great extent on the spin angle at which the tumble test takes place. The need to reduce spin errors before the tumble test could be resumed became obvious and we consequently focussed our attention on the spin errors.

7.3   Spin Orientation Test

Two main causes of spin errors were expected to exist; a) errors caused by magnetic inclusions; permanent and induced magnets and, b) errors caused by the misorientation of the H_1 field axis and the optical axis. In addition the presence of a spin error caused by AC magnetic field of the current passing through the heater wire was detected. We were able to reduce greatly the magnitude of this error by very tightly twisting the bifilar heater wire and by removing any current loops in the vicinity of the absorption cell.

The magnetic inclusion effects were still present. Be demagnetizing the sensor, their magnitude was reduced, but this was not sufficient. Two new sensor bodies were built out of fiberglass based tubes. The spin tests shown in Figure 14 and Figure 15 show spin errors of about 0.5 nT peak-to-peak. Magnetic inclusions causing these spin errors had to be isolated first and eliminated. The first step in this direction was the replacement of the resistive heater wire with pure copper wires. The spools of the resistive heater wire were tested and showed weak magnetic effects. A few more components like the thermistor, the photodiode and the lamp assembly were scrutinized. The rotation of the lamp assembly itself showed little effect, but the rotation of the photodiode assembly did. Two more photodiode assemblies with different photodiodes were built.

Some improvements were made in the orientation test setup: Longer cables (5 meters) were used between the sensor and the electronics rack in order to ensure that there was no possibility of magnetic interference from the rack. The photodiode assembly used previously in the sensor was found to be slightly magnetic and was therefore replaced with another completely non-magnetic
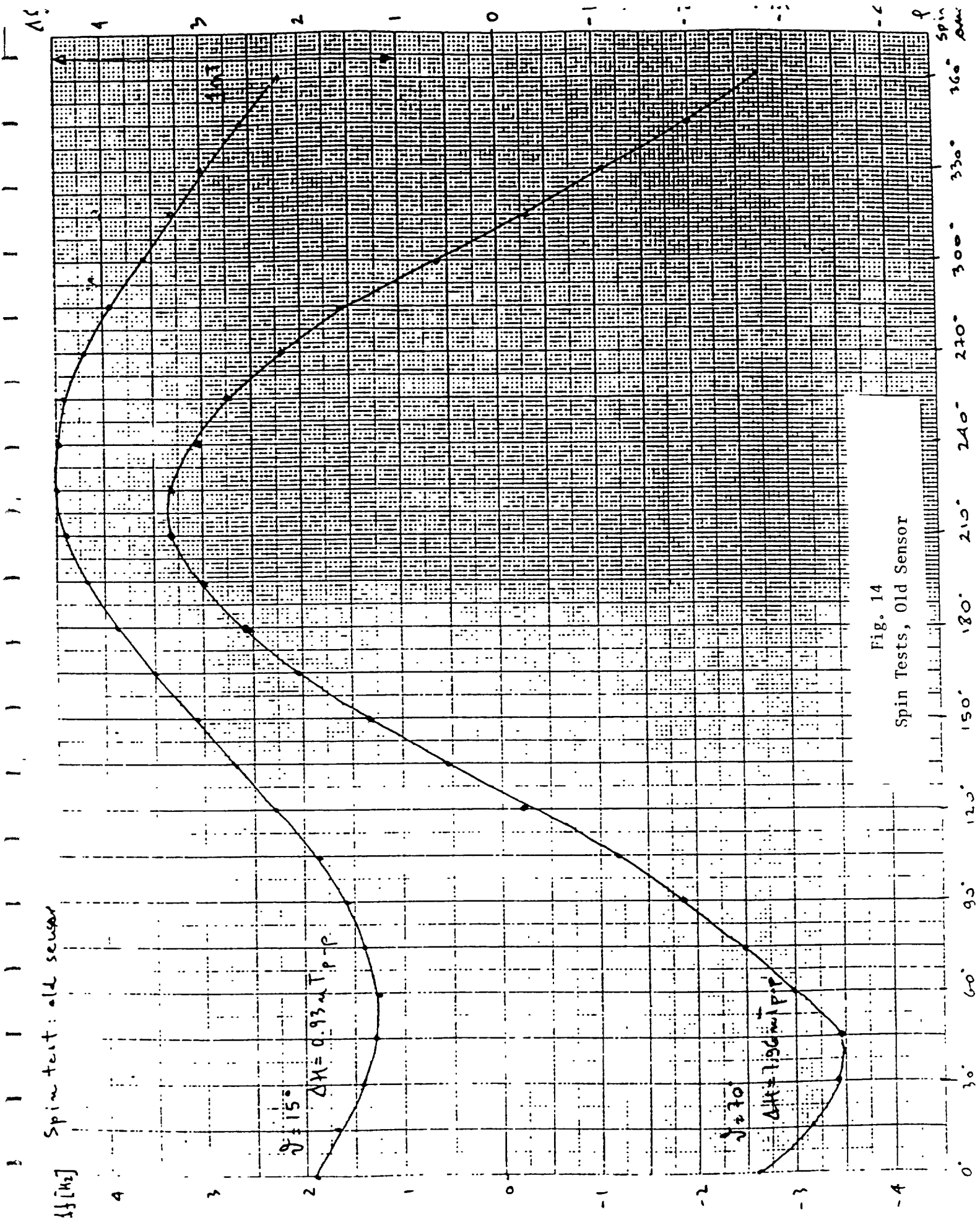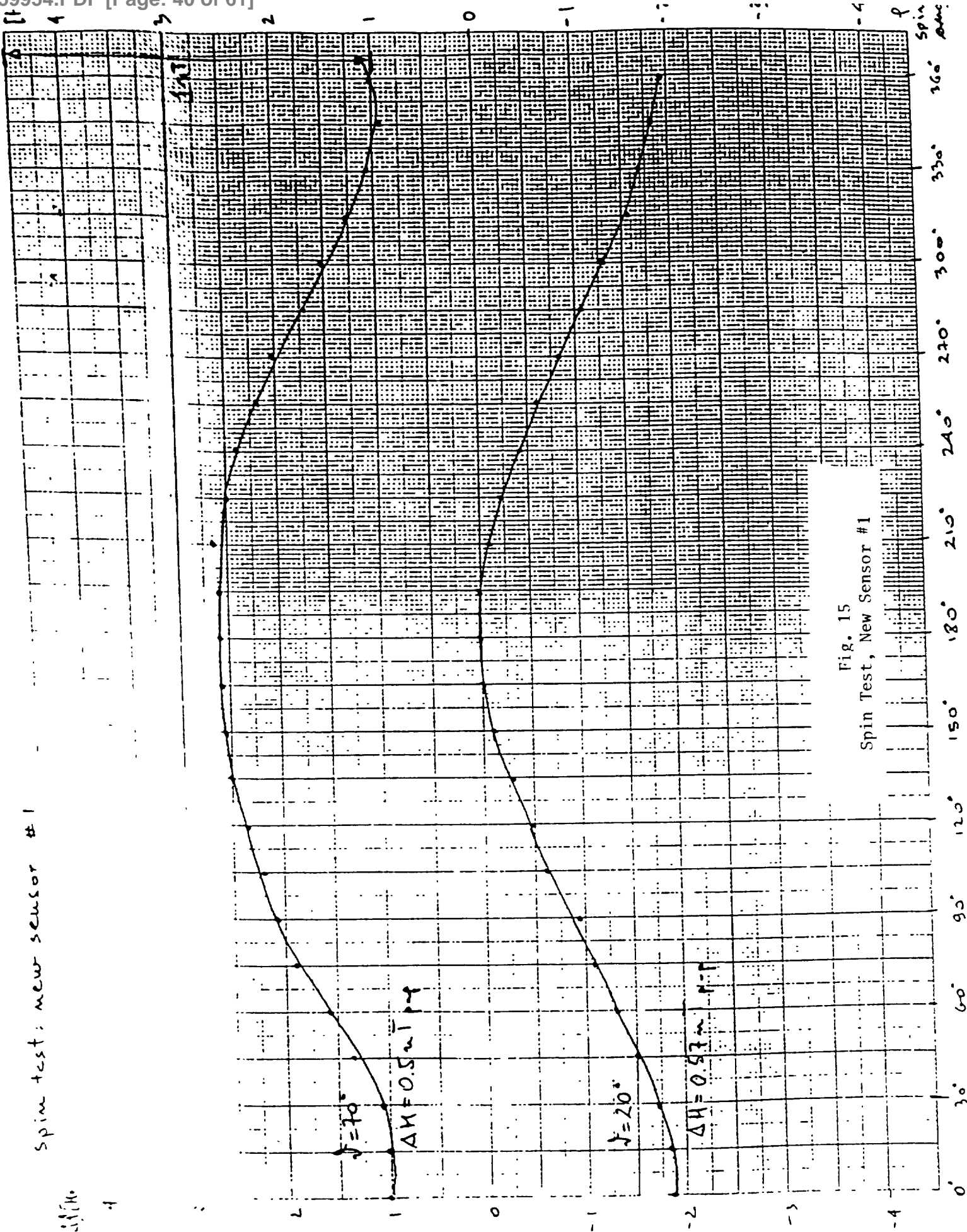
Fig. 14
Spin Tests, Old Sensor

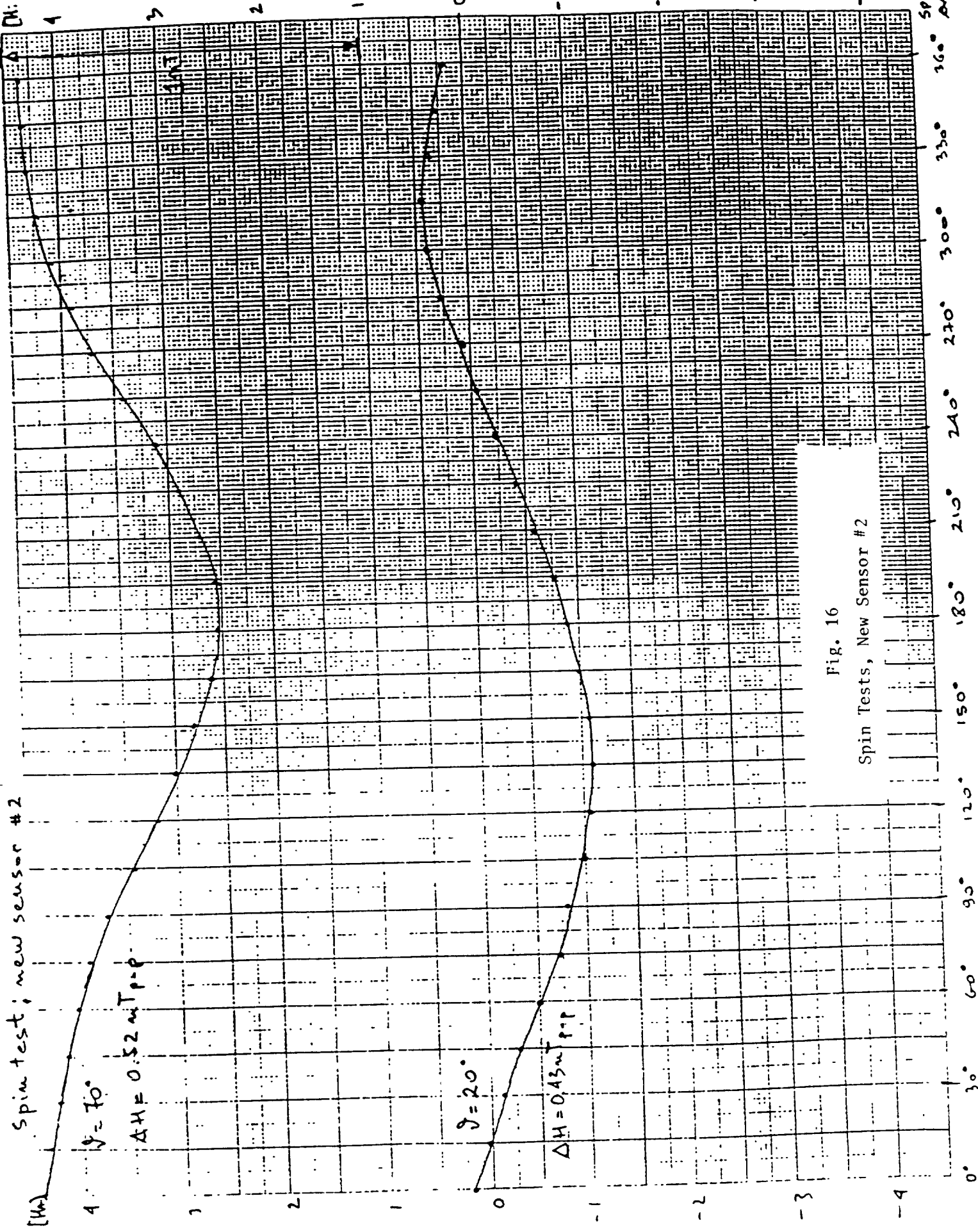Fig. 15
Spin Test, New Sensor #1

Fig. 16
Spin Tests, New Sensor #2

assembly. The sensor nichrome heater wire (also slightly magnetic) was replaced
with copper wire. Some small brass screws used in the photodiode assembly were
removed. The entire sensor was demagnetized to ensure that any remaining
magnetic impurities were demagnetized.

Spin tests at several different tumble angles were then conducted to verify that
the sensor was free of magnetic inclusions. The results are shown in
Figure 17. These spin tests indicated that the sensor was sufficiently free of
magnetic impurities that we could continue with tumble orientation tests.

7.4   Additional Tumble Orientation Tests

Tumble error still continued to be very large. We suspected that the error was
due to perturbation of the magnetic energy sublevels by the pumping light
i.e. "light shift". In order to determine if this was the case we conducted
tumble tests at different pumping light intensities. The light intensity was
adjusted by placing a circular aperture adjacent to the spectral lamp between
the lamp and the collimating lens to effectively reduce the size of the source
and thereby reduce the light intensity at the absorption cell as shown in
Figure 18. The results are shown in Figure 19. These curves clearly indicate
that the tumble orientation error increases with increasing light intensity.
Also evident from examining the curves is the fact that as the light intensity
is reduced so as to minimize the tumble error then the operating angular range
is restricted, due to the fact that beyond the limiting angle the pumping is not
sufficient to produce a significant population redistribution and the amplitudes
of the 4 absorption lines become nearly equal. When this happens oscillation
may take place at several frequencies simultaneously and simple frequency
counting techniques cannot be used to measure the frequency of interest.
Reduction of pumping light also reduces signal to noise ratio. Therefore simple
reduction of light intensity is not a viable means of reducing orientation
errors caused by light shifts.

The curves of Figure 19 also show evidence of line interaction effects at larger
tumble angles. As the tumble angle is increased the amplitude ratios of the
adjacent resonant lines approaches unity and the resonances adjacent to the
oscillating resonance tend to pull its frequency toward their region of the RF
spectrum (in this case toward lower frequencies). The line interaction effect
become greater at higher pumping light intensities because of the increase in
line width due to reduced life time. Hence the magnetometer operating frequency
falls below that corresponding to the "true" (no light shifts or line
interaction) magnetic field intensity value as the tumble angle approaches 90°
and the light intensity is increased. (See Section 4.3 for a discussion of line
interaction).

8.0   SENSITIVITY MEASUREMENT

Because the potassium magnetometer continued to demonstrate a serious tumble
error problem, we decided to see if the expected lower noise of the potassium
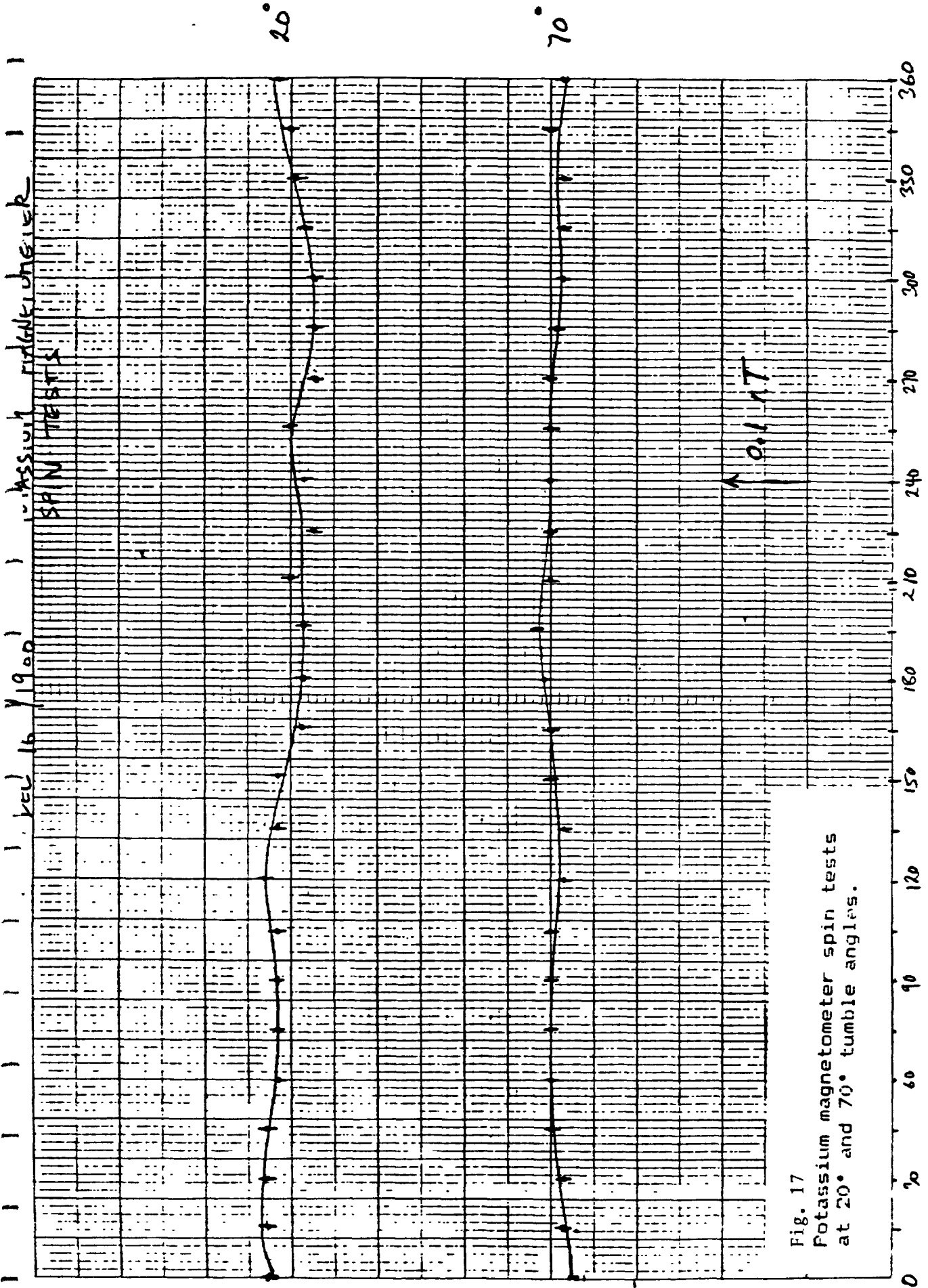magnetometer could justify further effort to reduce tumble error. The tests

Fig. 17
Potassium magnetometer spin tests
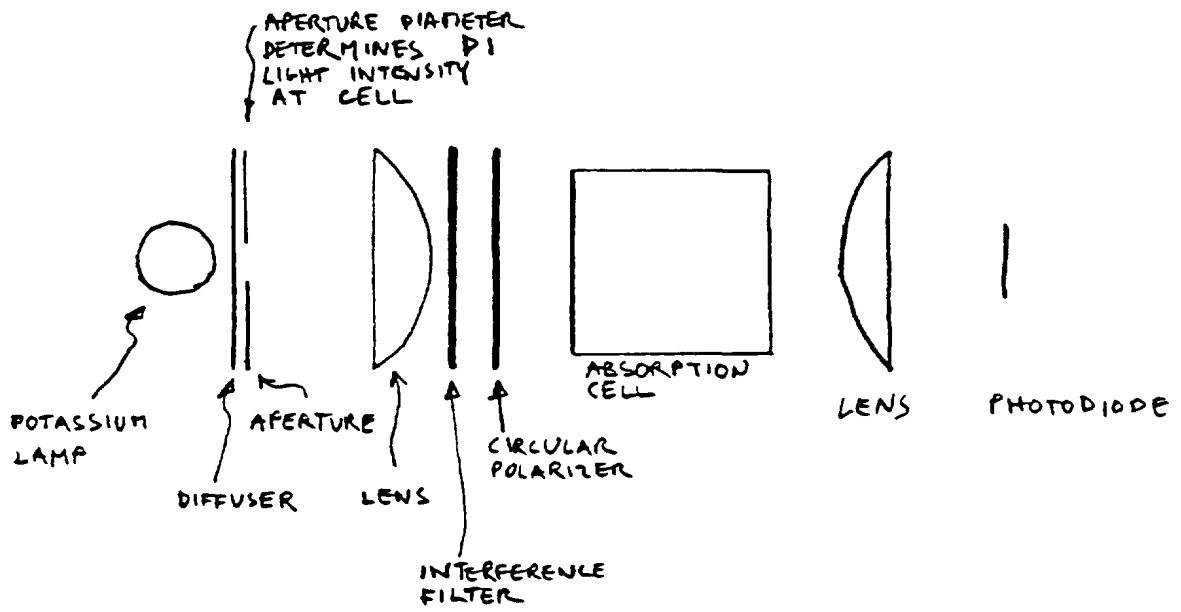at 20° and 70° tumble angles.

APERTURE DIAMETER
DETERMINES DI
LIGHT INTENSITY
AT CELL

POTASSIUM
LAMP

APERTURE

DIFFUSER

LENS

INTERFERENCE
FILTER

CIRCULAR
POLARIZER

ABSORPTION
CELL

LENS

PHOTODIODE
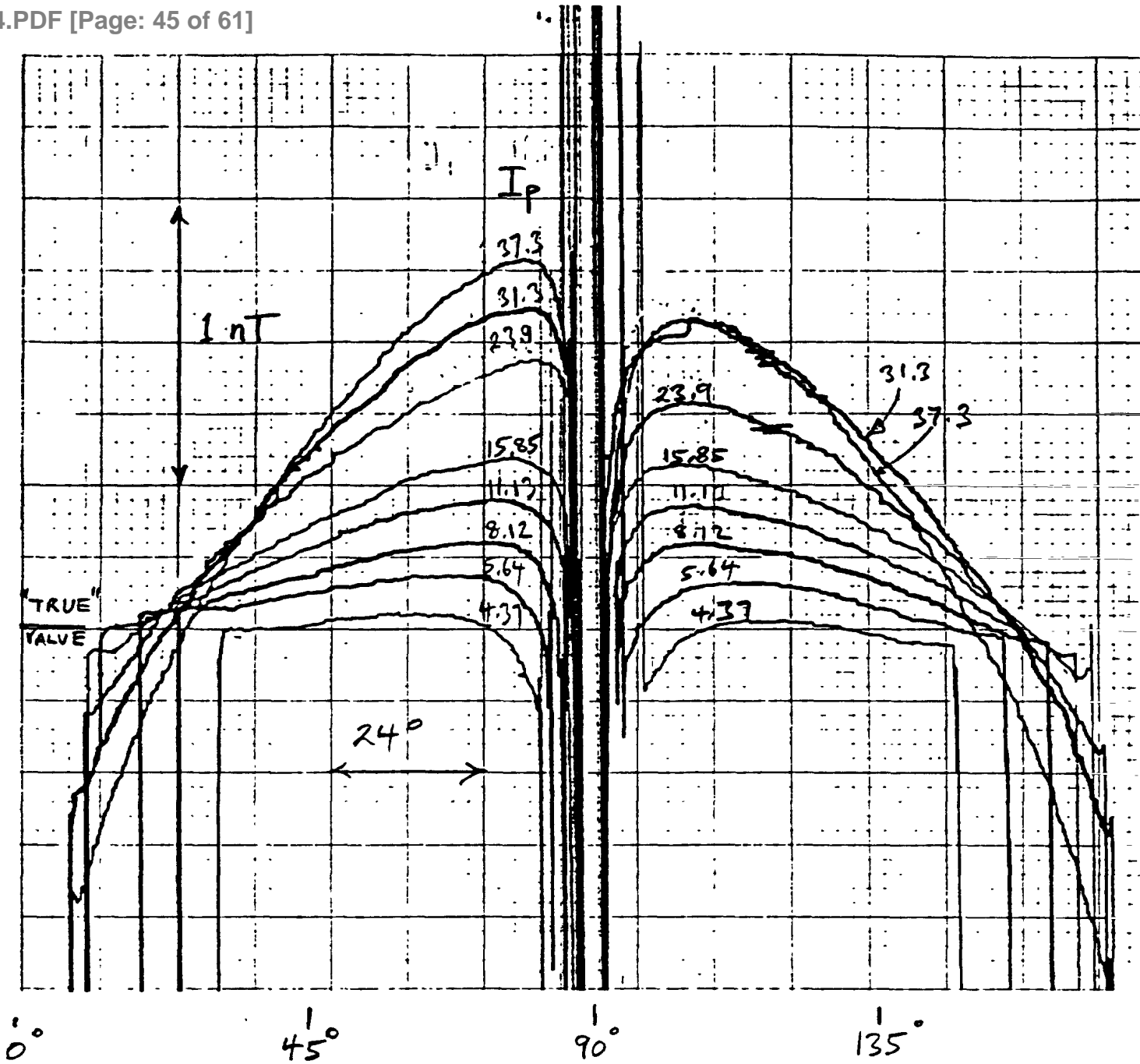
Fig. 18

Light shift experimental measurement setup.

Fig. 19
Magnetic field measurement value as
a function of tumble angle at different
pumping light intensities Ip (µW*cm-2)
for the potassium magnetometer.

Fig. 20

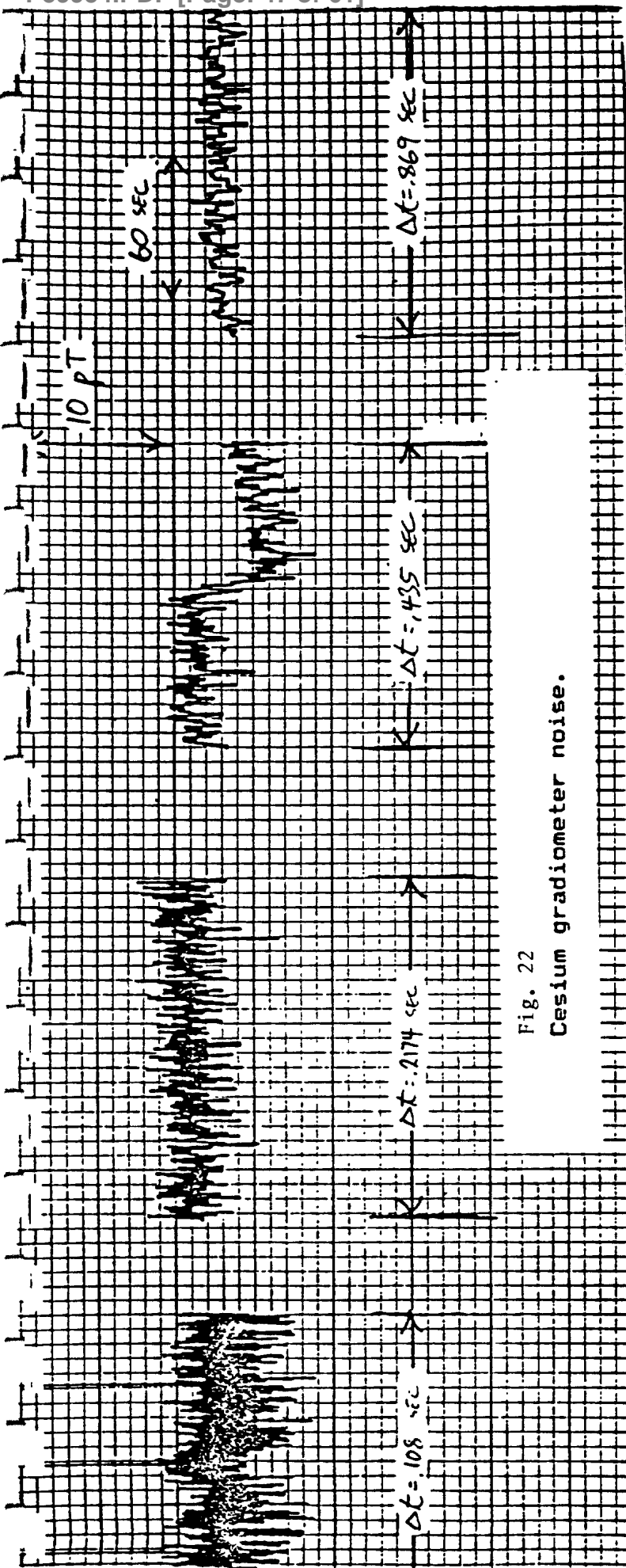Gradiometer setup for measurement of
magnetometer noise.

10 pT

60 SEC

Δt = .869 SEC

Δt = .435 SEC

Δt = .214 SEC

Δt = .108 SEC

Fig. 22
Cesium gradiometer noise.
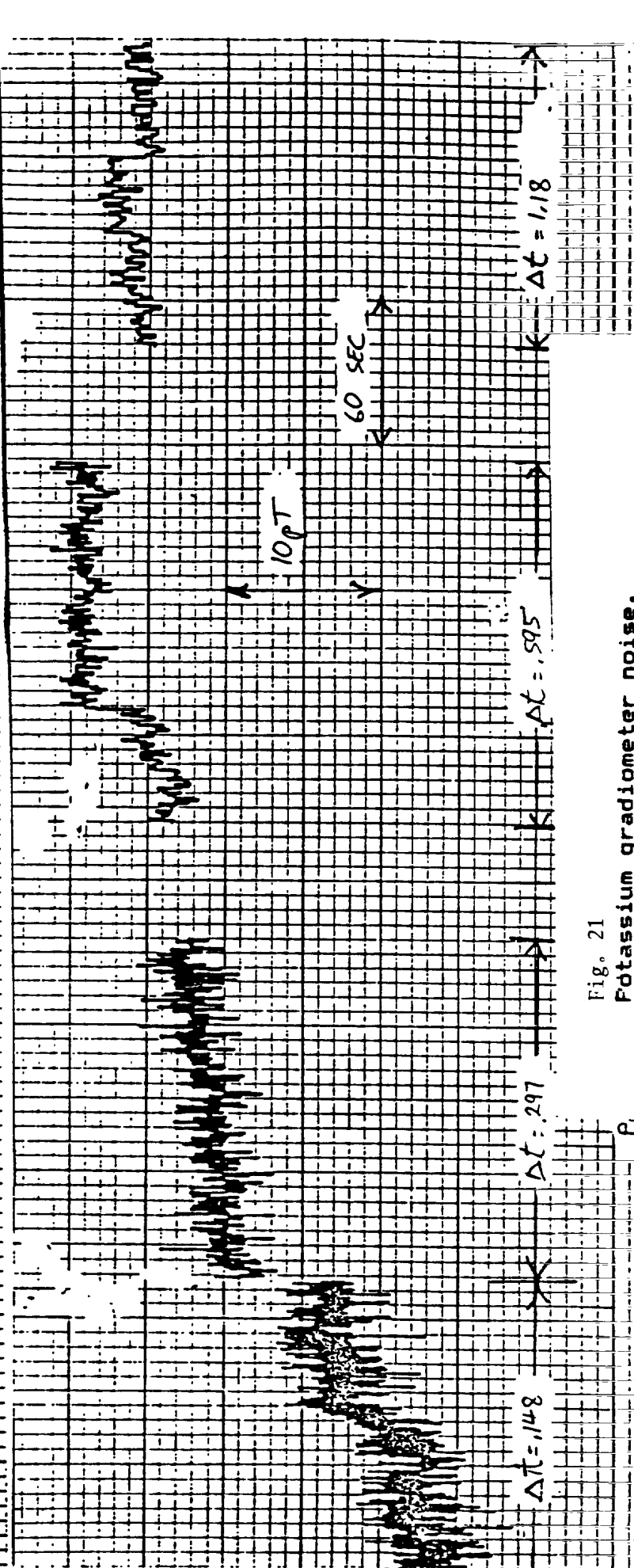
10 pT

60 SEC

Δt = 1.18

Δt = .595

Δt = .297

Δt = .148

Fig. 21
Potassium gradiometer noise.
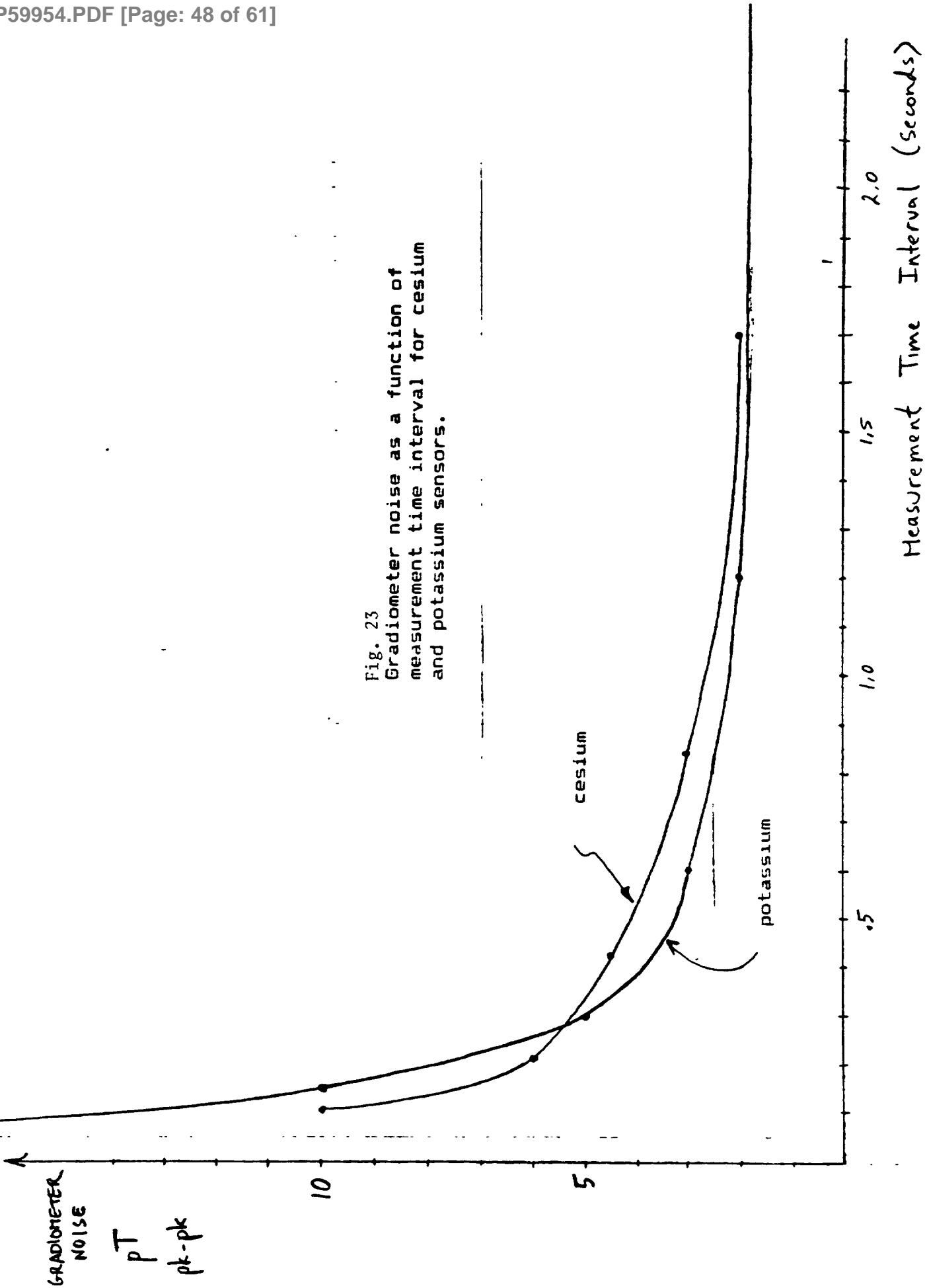
Fig. 23
Gradiometer noise as a function of
measurement time interval for cesium
and potassium sensors.

cesium

potassium

GRADIOMETER
NOISE

pT
pk-pk

10

5

Measurement Time Interval (seconds)

.5   1.0   1.5   2.0

consisted of comparing the noise level of two potassium sensors with that of two cesium sensors using the same oscillator electronics. The method used was to operate 2 identical magnetometers in a gradiometer configuration (Figure 20). The noise on the gradiometer measurement was then assumed to be due to magnetometer noise alone. Assuming the noise processes of the two sensors to be gaussion, uncorrelated and of equal variance we can determine the noise of one sensor by dividing by $\sqrt{2}$. The noise in a given measurement bandwidth can be determined by varying the count interval. A sample of the raw noise data is shown in Figure 21 for two potassium sensors operating as a gradiometer. Problems with potassium lamp stability prevented longer measurements. Similar data for two cesium sensors is shown in Figure 22. Gradiometer noise as a function of counter integration time is plotted in Figure 23 for cesium and potassium gradiometers. Equivalent noise bandwidth of the measurement is inversely proportional to the integration time. It is clear from this data that the potassium gradiometer does not have significantly lower noise than the cesium gradiometer.

9.0   STUDY OF DIFFERENT MAGNETOMETER EMBODIMENTS

One of our principal goals in a study of optically pumped magnetometers was a design of a system having significantly better orientational properties than presently built single beam magnetometer. Our study of a magnetic resonance in the $4^2S_{\frac{1}{2}}$ F=2 state of potassium indicated that systems working along the magnetic field or at a small angle to it, would have the desired properties. Therefore our attention was brought to two systems, described in the scientific journals as having these properties: 1) Cross beam magnetometer, 2) Locked oscillator magnetometer.

Both of the above systems have been studied in parallel with the time consuming program of orientation error measurements of the self-oscillating magnetometer. The cross beam magnetometer has been constructed and made operational. Because in a preliminary test, not very good results were obtained from the orientation tests of this magnetometer, and because we have obtained rather unexpected results of orientation error measurements from a single beam magnetometer (which are general enough to be valid for a cross beam system as well) we have decided to postpone further experimental studies on a cross beam magnetometer until we obtain a complete clarification and full understanding of the problems discovered. After the investigation of the self-oscillating magnetometer was complete, it became obvious that the same orientation problems would be encountered in the other two embodiments. For the completeness of this report, the results of the preliminary investigations for two alternate magnetometer embodiment are presented in this Section.

9.1   Cross Beam Magnetometer

A cross beam magnetometer, of which a block diagram is shown in Figure 24 is the closest in principle of operation and circuit design to a single beam magnetometer, that we have tested until now. Therefore, we have decided to test it first. Light emitted from the lamp 1 is collimated and circularly
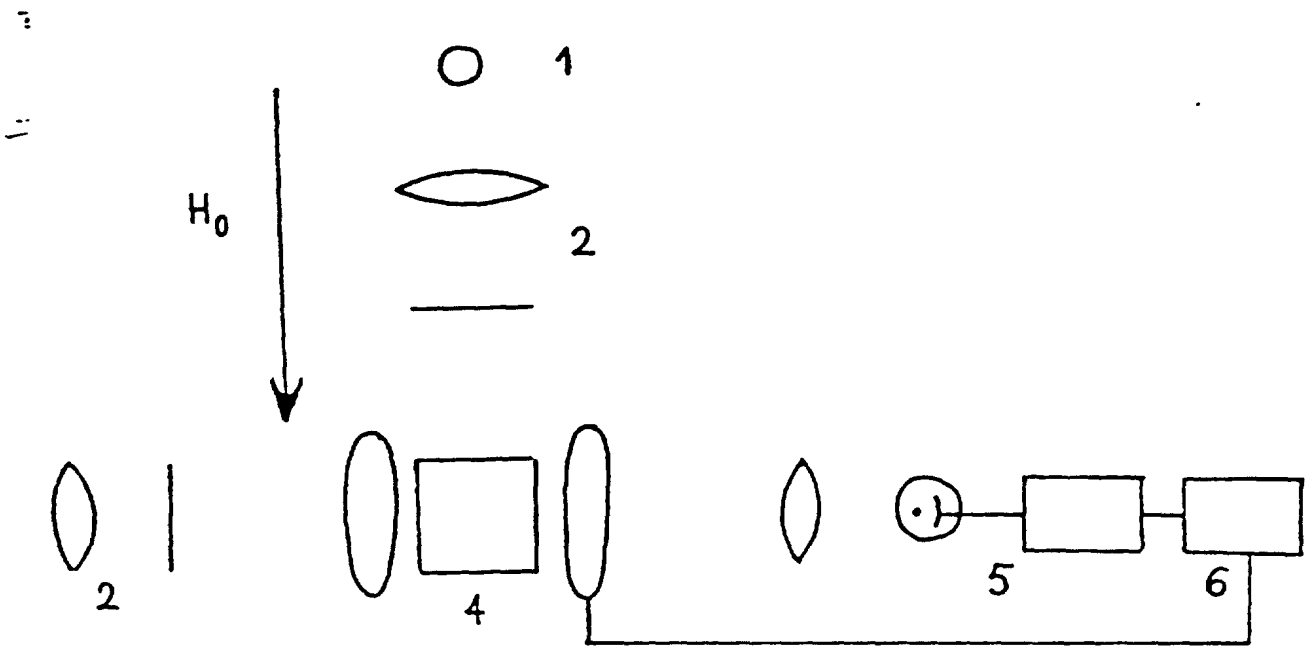
Fig. 24

Cross Beam Magnetometer

1. Pumping lamp

2. Optical system

3. Monitoring lamp

4. Gas cell and H_1 drive coils

5. Photodiode and Larmor amplifier

6. $\pi/2$ phase shifter

polarized. It orients potassium atoms along the magnetic field H_o. The signal
from the monitoring lamp 3, which is modulated in the gas cell 4, is amplified,
90° phase shifted, and is sent to the H_1 coils. When the frequency of the H_1
field coincides with the larmor frequency, the system operates as a self
oscillating magnetometer.

Ideally, intensity of the monitoring light beam should be nearly zero to satisfy
the condition of a weak signal (i.e. signal, which does not interact with
optically pumped atoms). However, for a practical reason (to keep the signal to
noise ratio high enough) the light intensity of the monitoring beam is almost as
high as intensity of the pumping beam. This results in a degradation of
performance of the magnetometer.

We have measured the following three parameters in this system:

1. Line width and line amplitudes ratio (of neighbouring resonances).

2. Signal amplitude in relation to the position of the magnetometer with
   respect to the magnetic field.

3. Orientation error of the magnetometer.

RE. 1: Line width of the magnetic resonance was about 20% broader than in a
single beam magnetometer. This is attributed to the fact that higher light
intensity was used in order to obtain a better signal to noise ratio and to make
a monitoring beam relatively weaker.

For the same reasons the ratio of the lines in a magnetic resonance spectrum was
not as good as expected. Line amplitude ratio changes from 4.8:1 to 2:1 in -60°
to +45° range. This is still better than in a single magnetometer, where change
from 5:1 to 1:1 was recorded in -70° to -15° and +15° to + 70° range.
Operational range of a cross beam magnetometer is also different: it covers
-52° to +38° without the polar dead zone rather than ±15 to 70°) with the dead
zone as in the case of a single beam magnetometer.

RE. 2: When the magnetometer is rotated along the monitoring beam axis (that is
when the monitoring beam remains perpendicular to the direction of the magnetic
field) the signal amplitude is shown in Figure 25a and is as predicted in many
publications. However, if we rotate the magnetometer around the axis which is
perpendicular to the pumping and monitoring beam axis, the signal amplitude
becomes highly asymmetric (with respect to the magnetic field direction) and is
shown in Figure 25b. This result may be easily explained, by analyzing the
pumping and monitoring light contribution to the whole optical pumping cycle.
(See Figure 26).

Both monitoring and pumping optical systems are equipped with ς^+ circular
polarizers. When a cross beam sensor is placed in such a way that both beams
are propagating in the same direction with respect to the magnetic field, then
both of them are pumping potassium vapour in a gas cell (Figure 26a). However,
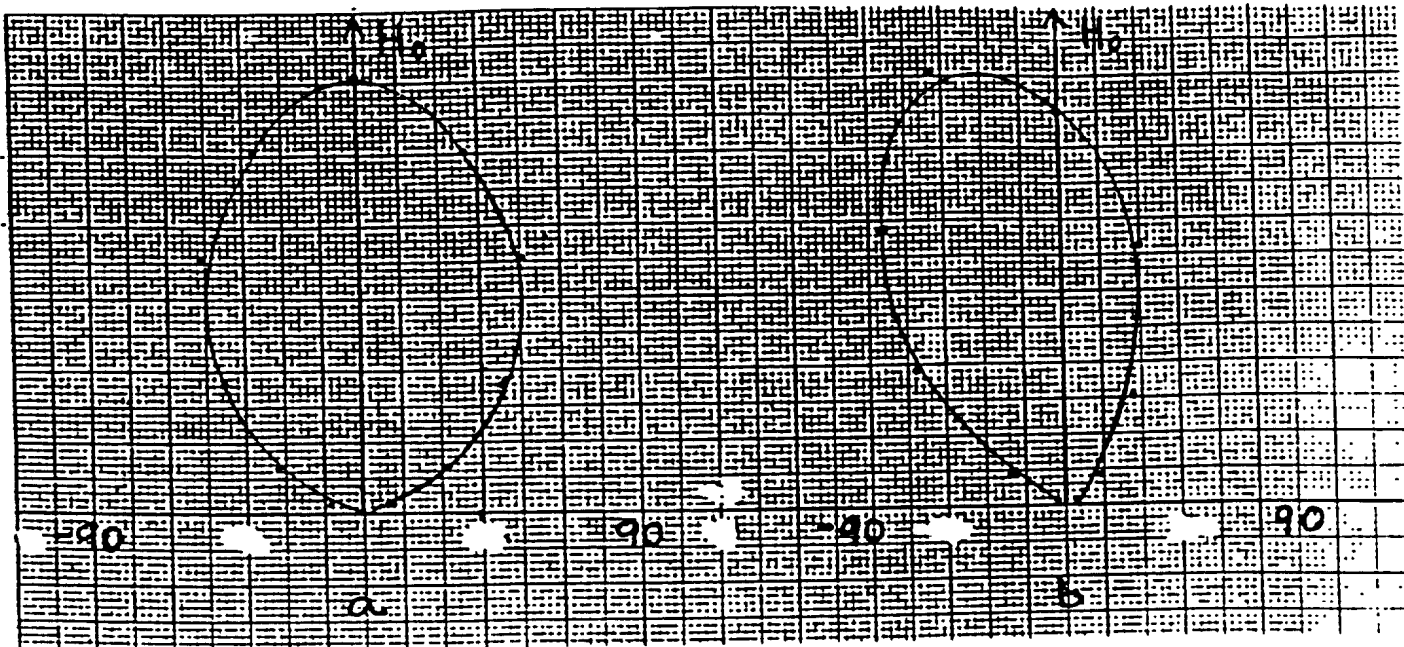when a sensor is placed as shown in Figure 26b then the monitoring beam,

Fig. 25

Signal amplitude VS tumble angle for two spin angles 90° apart

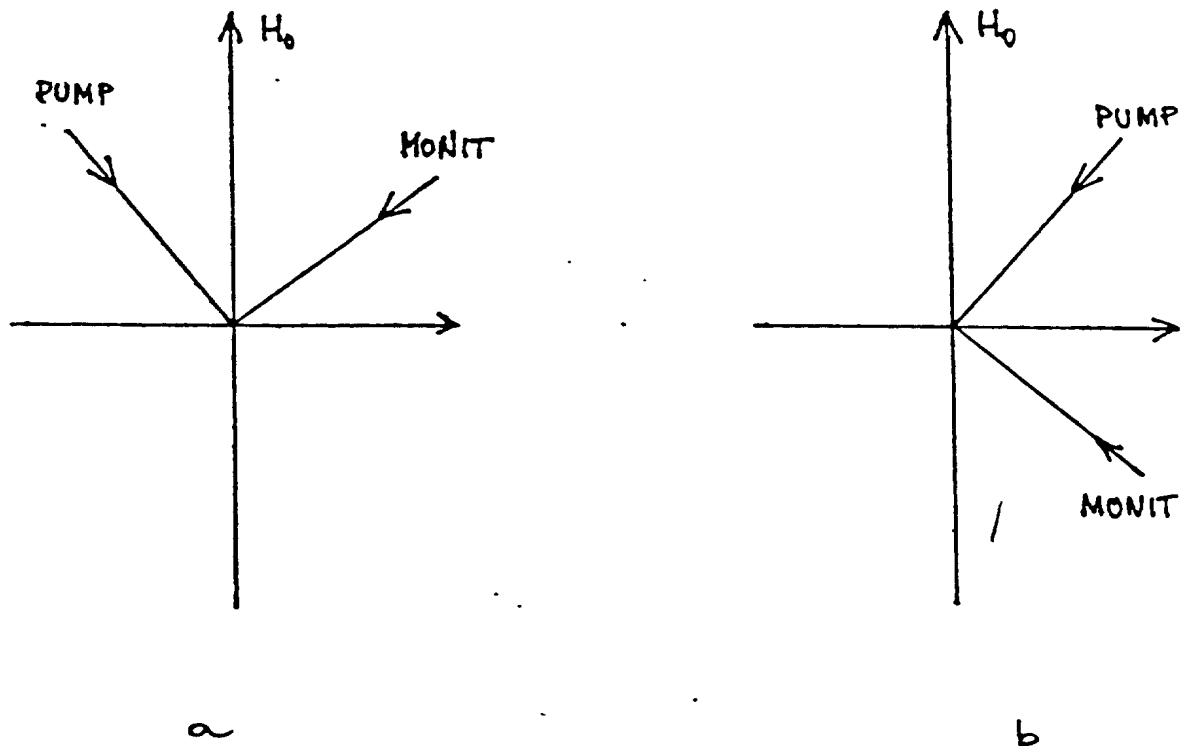a   b

Fig. 26

Different pumping and monitoring light geometries

propagating in the opposite direction to the pumping one, depumps the system, and destroys the achieved orientation, thus limiting the useful operation range of the instrument. This was observed, to our knowledge, for the first time.

RE. 3: The performance of a cross beam magnetometer was somewhat disappointing. Orientation error in the northern and southern hemisphere was nearly the same magnitude (± 0.5 and ± 0.45 nT respectively). See Figure 27.

At the time of this measurement, we did not know if this orientation error was caused by some magnetic impurities in a sensor, or whether it is inherent to the system itself.

In conclusion, it became clear during our experiments that the signal amplitude in a cross beam magnetometer is by far more complicated than has been reported to date in the available literature. The importance of this finding lies in the fact that under certain conditions, spinning of this type of a magnetometer about its optical axis changes its reading and nothing can be done about it, because it originates in the various types of frequency shifts which are described in Section 7.1.2. This poses a serious limitation on this type of a magnetometer, because it will require preorientation for high precision performance. The orientation error performance caused by the light shift effects could not be any better than in self-oscillating magnetometer. A cross beam magnetometer is also mechanically much more complex and difficult to design as it consists of two light beams, perpendicular to each other; therefore the placing of various components (like heaters, temperature sensors, H_1 drive coils, etc.) is much more critical, as they have to be place relatively close to the gas cell and at the same time cannot obstruct the light paths and must not interfere with each other.

9.2   Locked Oscillator

In the locked oscillator magnetometer (M_z magnetometer) the optical axis is directed along the field direction. A tunable oscillator provides a high frequency signal fo to H_1 coils orthogonal to the optical axis. When this signal is at a resonance frequency the light incident on the photodiode is at a maximum. A sinusoidal frequency or phase modulation of f_o with small peak excursion of f at a low frequency f_m leads to a modulation of the light intensity at the photodiode with frequency components of fm and harmonics of f_m. This light modulation signal is amplified and synchronously detected with the oscillator modulation signal as phase reference. The synchronous detector output provides an error signal which provides feedback to tune the oscillator to the resonance frequency. When the oscillator is at resonance, the system is said to be locked.

There are several difficulties inherent to the locked oscillator system:

1) Lock Acquisition:

When the oscillator is not locked (initial condition after turn on) no modulation of the light intensity at the photodiode is present and no error
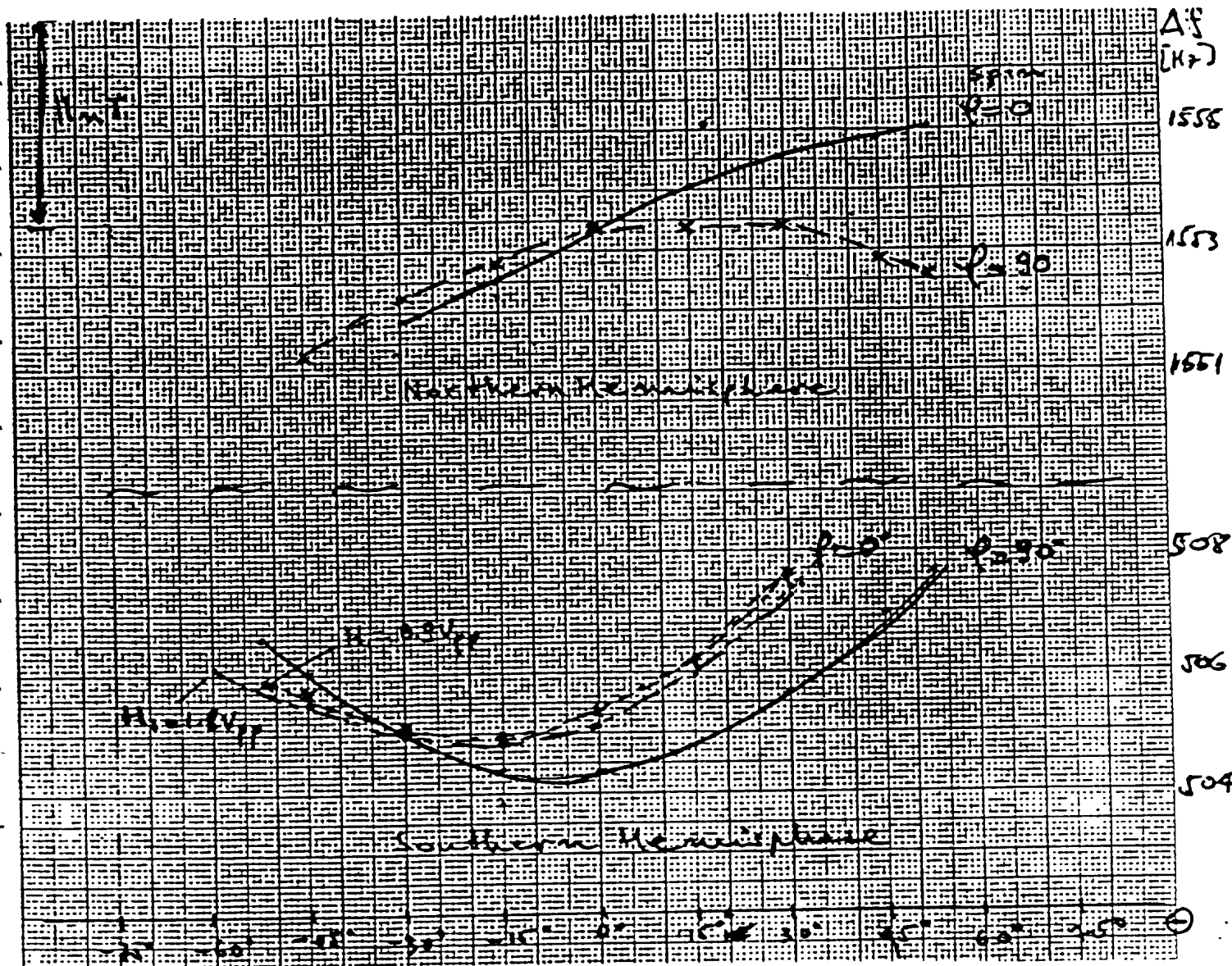
signal is available to adjust the oscillator frequency to resonance. An
auxiliary circuit is therefore required to open the feedback loop and slowly
sweep the oscillator across its frequency range until an error signal is
detected at which time the loop is closed and the system locks. If we assume
that the maximum allowable frequency sweep rate is such that the oscillator
center frequency fo falls within the passband of the resonance for a time equal
to the time constant of the resonance then we find that:

$$\frac{df_o}{dt} \quad max = \pi f_B^2 \text{ Hz/sec.}$$

where f_B is the resonance bandwidth.

A typical resonance line width is 35 Hz (5 nT)

Therefore $\quad \dfrac{df_o}{dt} \quad max = \pi 35^2 = 3.850 \text{ KHz/sec.} = 550 \text{ nT/sec.}$

In a typical system the oscillator frequency range would be about 560 KHz
(80 μT). Thus the lock acquisition time could be as long as 145 seconds.

A further difficulty with a locked oscillator using potassium is that caused by
the 4 distinct closely spaced resonances. The system would have to always lock
to the same resonance, for example the highest frequency of the four. Fairly
sophisticated electronics would be required to ensure that the system does not
lock to, say, the 2nd highest resonance, if for example the measured field
suddenly increased by an amount equal to the resonance line separation.

2) Rate of Change of H_o Field:

Because of the long time constant required to filter the synchronous detector
output ripple the locked oscillator will not be able to follow (track) a rapid
rate of change of resonance frequency due to changing Bo field. The maximum
rate of change would have to be less than f_B^2 in order for the system to
maintain lock. A typical maximum rate would therefore be 3.85 KHz/sec.
(550 nT/sec.).

3) Counting Error

The process of counting the oscillator frequency for a duration Δt is equivalent
to computing the time average of the frequency.

If the oscillator is frequency modulated then the oscillator instantaneous
frequency has the form.

$$f_i = f_o + \Delta f \cos 2 \pi f_m t$$

The average value of frequency is:

$$f_{av} = \frac{1}{\Delta t} \int_{o}^{\Delta t} t \ f_1 dt$$

$$f_{av} = f_0 + \frac{\Delta f}{2\pi f_m \ t} \ \sin 2 \ \pi f_m \Delta t$$

The second term is an error term. It can be completely eliminated by choosing Δt and f_m such that $f_m \ \Delta t = n$, $n = 1,2,3$

This places additional restrictions on acceptable values of f_m and Δt, which often can not be fulfilled in practice.

10.0   REASSESSMENT OF POTASSIUM MAGNETOMETER POTENTIAL

The results obtained in our experimental investigations revealed some significant shortcomings intrinsic to the potassium magnetometer. These are listed below:

10.1   Line Interaction

As outlined in Section 4.3, for a given line width of the potassium absorption spectrum, the effects of line interaction on the orientation error of the magnetometer become increasingly severe as the total magnetic field is reduced. The only obvious way to reduce these orientation errors is by reduction of the line width. Reduction of the line width would require a painstaking R&D program to investigate the effects of cell volume, buffer gas types and pressures, cell wall coatings, etc. on the line width. However, it is not clear whether or not the line width could be sufficiently reduced in a practical magnetometer so that line interaction effects at low field strengths could be ignored. Evidence of line interaction effects at 57000 nT strength has been confirmed by experiment in the light intensity experiments shown in Figure 19.

Based on our line interaction mathematical model we expect more orientation error due to line interaction at lower field strengths, although this is difficult to confirm experimentally due to the difficulty in generating a low gradient low intensity magnetic field.

10.2   Light Shift

At the field intensity which exists at the Scintrex test site the light shift induced orientation errors dominate the line interaction errors. Reduction of light shifts by reduction of D1 light intensity is not a satisfactory solution because of the accompanying degradation of signal to noise ratio. No more satisfactory technique for compensation or reduction of light shift has been suggested up until the time of this report.

10.3   Potassium Lamps

Electrodeless discharge lamps based on potassium are very difficult to build
because of the problem of degradation of the glass envelope by the potassium.
This is due to the great affinity of potassium for oxygen. Since all glasses
contain oxygen, the potassium tends to migrate into the surface layer of the
envelope and form sub-stoichiometric compounds with the oxygen atoms. The
formation of these compounds results in blackening of the envelope and a
reduction in light output. It is thought that a polymeric coating of zirconium
on the glass surface might prevent this degradation but this has not yet been
attempted.

The lamps which were constructed tended to be unstable and of relatively short
lifetime. Attempts to improve stability and lifetime by the addition of a
temperature controlled potassium reservoir were met with limited success.

11.0   CONCLUSIONS

Because of the serious difficulties explained in Section 10, the further
development of the potassium search mode magnetometer has been discontinued. We
do not consider the obtained performance satisfactory to propose the
continuation of the program based on potassium magnetometer into Phase 3.
However, we have continued the search funded internally by Scintrex to
reevaluate the cesium magnetometer. Most of the instrumentation developed and
especially the experience gained in investigating the potassium magnetometer can
be applied to the cesium magnetometer investigation.

In order to facilitate experiments with the cesium magnetometer, a new sensor
assembly was constructed incorporating features designed to allow easy
interchange of components and reconfiguration of the sensor so that the
experiments can be conducted easily and modified quickly. The assembly is
somewhat similar to a small optical bench. Orientation tests were then
conducted for a split beam cesium sensor. Some typical results for spin and
tumble tests are shown in Figure 28 and 29. These results are very encouraging
and have led us to propose a program to achieve this low orientation error
performance in a production sensor.

SPLIT POLARIZER
7u PLATE # 2

GAIN FIELD α=0
Bk HEATER OFF $T_A = 22°$

SPIN TEST AT DIFFERENT TUMBLE ANGLES

FREQUENCY TO VOLTAGE CONVERTER $\eta = 4$
FOR θ = 45 & 70 $\eta \sim 16$ FOR θ = 20

$I_{osc} = 250$ mA

CELL TY = 50 TORR N_2 GLASS 1 IN in SIDE

HN 22

1 nT

θ: 70 45 20

Fig. 28
Magnetic field measurement value as
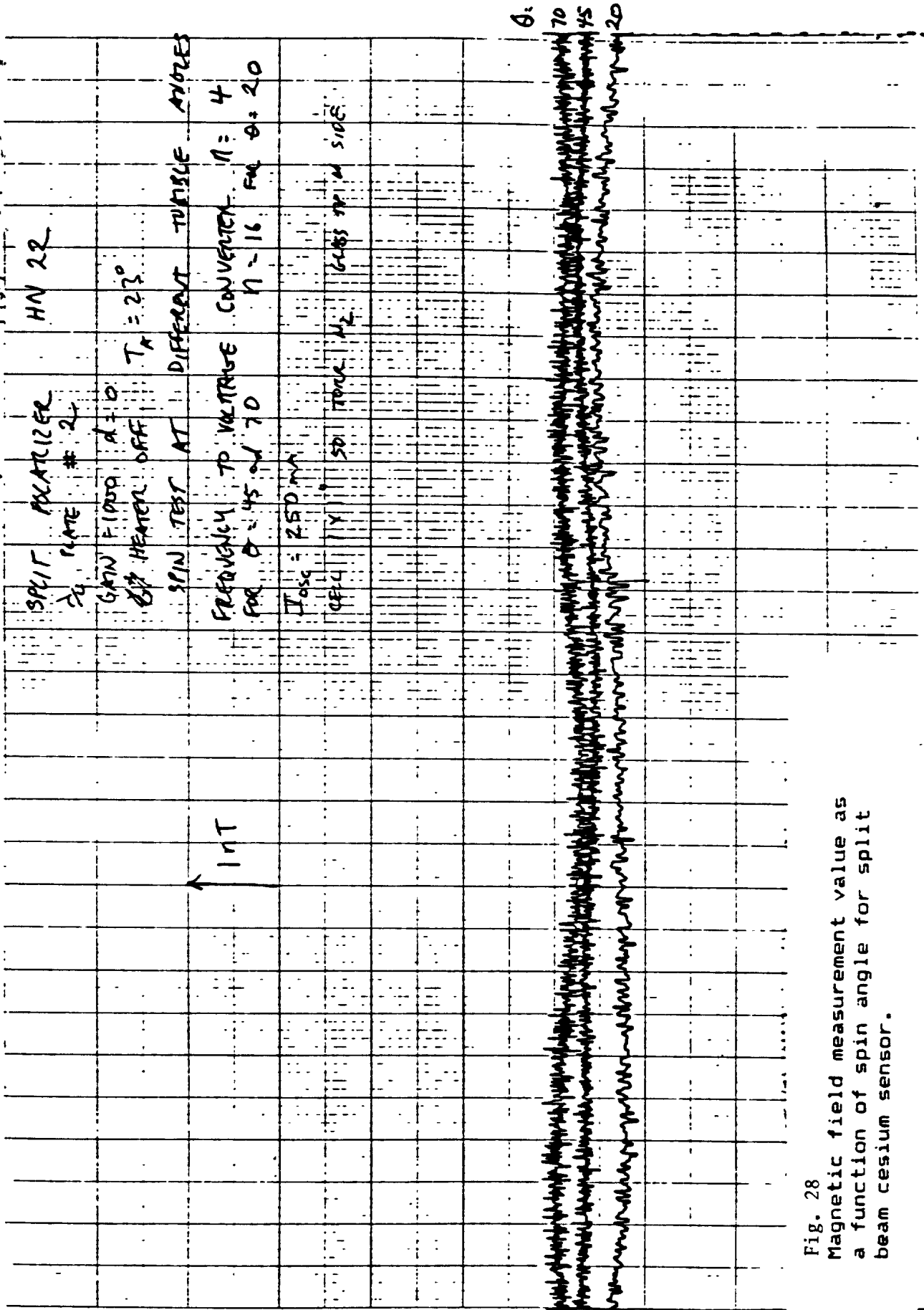a function of spin angle for split
beam cesium sensor.

Fig. 29
Magnetic field measurement value as
a function of tumble angle for split
beam cesium sensor.

26

12.0   REFERENCES

Bell, W.E. and Bloom, A.L., Phys. Rev. 107,1559 (1957)

Bloom, A.L., Appl. Opt. 1, 61 (1962)

Cohen, C. – Tannoudji, Ann. Phys. 7, 423 (1962); 7,469 (1962)

Dehmelt, H.G., Phys. Rev. 105, 1487, 1924 (1957)

Malnar, L., Mosnier, J.P., Ann. Radioelec., 16, 63 (1961)

Mathur, B.S., Tang, H., Happer, W., Phys. Rev. 171, 11 (1968)

Schearer, L.D., Advances in Quantum Electronics (Colombia University Press, New York 1961).

Slocum, R.E., Rev. Phys. Appl. 5, 109 (1970)

Usher, M.J., Stuart, W.F., J. of Phys. E, 3, 203 (1970)

Yabuzaki, T., Tsukola and T. Ogawa, Japan J. Appl. Phys. 11, 10/1 (1971)

Yabuzaki, T., Ogawa, T., J. of Appl. Phys. 45, 1342 (1974)

RD/IB-3/14

UNCLASSIFIED

MAY 26 1989

NO. OF COPIES NOMBRE DE COPIES	COPY NO. COPIE N°	INFORMATION SCIENTIST'S INITIALS INITIALES DE L'AGENT D'INFORMATION SCIENTIFIQUE
1	1	AS

#59954

AQUISITION ROUTE FOURNI PAR ►	DRES
DATE ►	23 MAY 1989
DSIS ACCESSION NO. NUMÉRO DSIS ►	89-02041

DND 1158 (8-87)

▮✦▮ National Défense
Defence nationale

PLEASE RETURN THIS DOCUMENT   PRIÈRE DE RETOURNER CE DOCUMENT
TO THE FOLLOWING ADDRESS: À L'ADRESSE SUIVANTE:

DIRECTOR
SCIENTIFIC INFORMATION SERVICES
NATIONAL DEFENCE
HEADQUARTERS
OTTAWA, ONT. - CANADA K1A 0K2

DIRECTEUR
SERVICES D'INFORMATION SCIENTIFIQUES
QUARTIER GÉNÉRAL
DE LA DÉFENSE NATIONALE
OTTAWA, ONT. - CANADA K1A 0K2

UNCLASSIFIED